PHYSICAL REVIEW D

PARTICLES AND FIELDS

THIRD SERIES, VOLUME 29, NUMBER 1 1 JANUARY 1984

Cosmic-ray muon spectrum up to 20 TeV at 89° zenith angle

S. Matsuno, F. Kajino, Y. Kawashima, T. Kitamura, K. Mitsui, Y. Muraki, Y. Ohashi, A. Okada, and T. Suda
Institute for Cosmic Ray Research, University of Tokyo, Tanashi, Tokyo 188, Japan

Y. Minorikawa
Department of Physics, Kinki University, Higashi Osaka, Osaka 577, Japan

K. Kobayakawa
College of Liberal Arts, Kobe University, Nada-ku, Kobe 657, Japan

Y. Kamiya and I. Nakamura
Department of Physics, Nagoya University, Chikusa-ku, Nagoya 464, Japan

T. Takahashi
Department of Physics, Osaka City University, Sumiyoshi-ku, Osaka 558, Japan

(Received 1 June 1983)

The 800-ton cosmic-ray spectrograph (MUTRON) has been used to measure the sea-level energy spectrum of cosmic-ray muons arriving from 86° to 90° zenith angles in the momentum region of 100—20 000 GeV/c. The measured muon energy spectrum can be interpreted by using a cosmic-ray primary spectrum of $(1.80\ \mathrm{cm}^{-2}\mathrm{s}^{-1}\mathrm{sr}^{-1}\mathrm{GeV}^{-1})E^{-2.70}dE$ (E in GeV) and a scaling model incorporating an increasing interaction cross section for meson production in hadron-hadron interaction. The muon charge ratio at energies up to 15 TeV in the same zenith-angle range has been measured. It shows a small enhancement with increasing energy. By combining both results we may conclude that the cosmic-ray primary particle composition stays the same up to about 100 TeV as that obtained by direct measurements in the energy range below 1 TeV.

I. INTRODUCTION

The cosmic-ray muon spectrum at sea level is one of the most important quantities for cosmic-ray investigations. The muon spectrum carries information[1] on the nature of the primary spectrum[2] and on the elementary-particle interactions at high energies. The spectrum reflects the parent-meson spectra (pions and kaons)[3] in the atmosphere and can be related to the primary galactic nucleon spectrum by extrapolating the interaction properties of hadrons from the accelerator energy range up to higher energies. Also, by comparing the muon spectrum at sea level with the underground range spectrum, electromagnetic muon interactions including inelastic interactions with nuclei have been studied[4] beyond the energy range of accelerator-produced muons.

For the measurements of the muon spectrum, three methods have been used: first, the direct method by a magnet spectrometer,[5] second, an indirect method by cascade showers,[6] and third, underground range measurements.[7] While the underground range measurements extend to higher muon energies, they suffer from uncertainties in the muon interactions in the rock. The burst-size measurements have given[8] inconsistent results about the spectral index of the muon energy spectra. Since the direct measurements by magnet spectrometers are limited by the resolving power and acceptance of the spectrometers used, the measurements in the past have been restricted to muon momenta around 1 TeV/c. We have taken an attempt to extend the range of direct muon momentum measurements by constructing a large magnetic spectrometer named MUTRON,[9—11] a solid-iron magnet spectrometer weighing 800 tons and a calorimeter including 120 tons of iron target. The maximum detectable momentum (MDM) of the magnet spectrometer is 22 TeV/c, which is the world's highest MDM at present. The momentum spectrum and charge ratio of cosmic-ray muons have been measured by the magnet spectrometer while the details of interactions of muons of known momenta have been studied in the calorimeter. All muons above a certain threshold energy E_c are produced by primary nucleons with a median energy of about (6—10) E_c.[12] Thus, the muon momentum range can cover the primary energy region of above 10^{12} eV to about 2×10^{14} eV and can give information on interaction properties of hadrons in that same energy region.

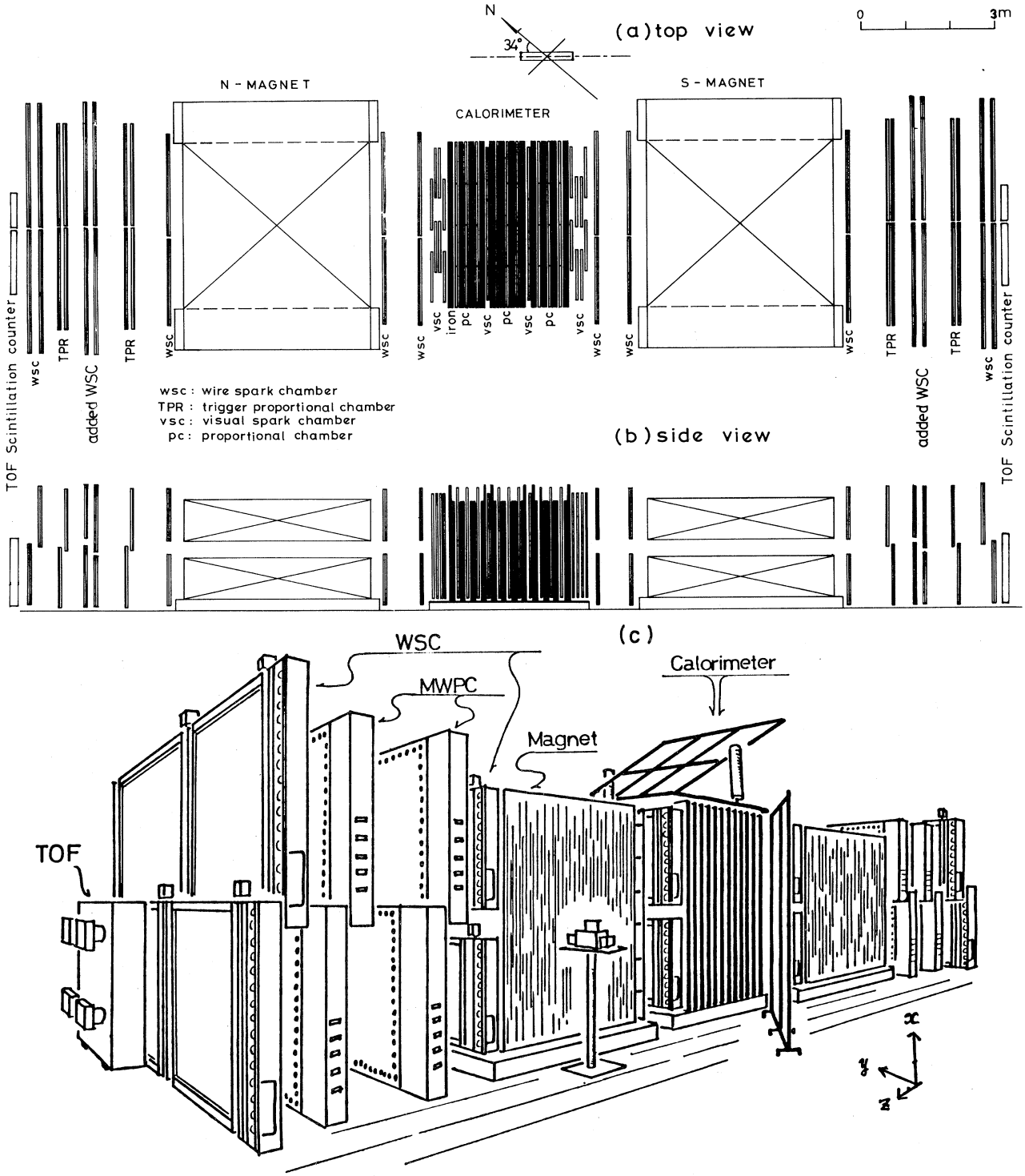

FIG. 1. (a) and (b) Side and top views of MUTRON. Four air-shower trays, each one being a 50×50-cm plastic scintillator, are located above the calorimeter at a height of 6 m. (c) A three-dimensional view of MUTRON.

Very recently, the $p\bar{p}$ collider storage ring at CERN[13] has provided data of interactions at equivalent laboratory energies of 155 TeV. The data, however, are restricted mainly to the central region of interactions and do not really cover the fragmentation region which is essential for the propagation of secondary particles in the atmosphere. Also the real problem treated at the $p\bar{p}$ collider is $p\bar{p}$ collisions, while in cosmic rays we are dealing with p-air or nucleus-nucleus collisions. Thus, the muon spectrum measured by the MUTRON spectrometer can give

better information on hadron—air-nucleus interactions around the 10^{14} eV energy region, supplementing the collider data.

The Japanese-American cooperative emulsion experiment[14] (JACEE) is also providing data where they can distinguish between different nuclei for cosmic-ray primaries above 10^{12} eV and up to several 10^{14} eV by a direct method using the emulsion chamber. The measured energy region overlaps with that of the primary spectrum derived from the present muon spectrum. It will be possible to derive the primary spectrum from both data sets more precisely.

II. APPARATUS

A. General characteristics

The MUTRON arrangement consists of a solid-iron magnet spectrometer and a calorimeter. The top and side views of MUTRON are shown in Fig. 1 and the characteristics of the spectrometer in Table I. The magnet spectrometer consists of two 400-ton solid-iron magnets used to deflect muons, four layers of 20 multiwire proportional chambers (MWPC's) for triggering, and 12 layers of 48 (196 channels) magnetostrictive-readout-type wire spark chambers (WSC's) for locating the muon trajectory position with an accuracy of better than 1.0 mm. The two magnets are located 626 cm apart and each magnet is made of about 400 tons of iron, its length, height, and width being 424, 240, and 600 cm, respectively. The central gap of the magnet is 40 cm high and 400 cm wide. The $\int B\,dl$ is 1.32×10^7 G cm for the two magnet blocks combined. As a result, the muon momentum is given by $p=(3.96/\theta)$ GeV c^{-1}, where θ is the muon deflection angle expressed in radians.

The MUTRON is set up as a horizontal spectrometer because the muon flux above 1 TeV has its maximum value in that direction, i.e., more than three times compared to the vertical one, and we are interested in a measurement of the muon spectrum and a study of the interactions of muons in the energy region, in which accelerator muon beams have not yet been available. The zenith-angle range of the incident muons is 86°—90°. The acceptance of the spectrometer including the WSC system varies with muon momenta and their entire angle of incidence. A Monte Carlo calculation has been performed to obtain the acceptance-correction factors as functions of momentum and zenith angle. The aperture of the spectrograph is 1280 cm^2 sr for momenta >0.2 TeV.

The calorimeter has dimensions of $4.0\times3.6\times2.4$ m and is set between the two solid-iron magnets of MUTRON as shown in Fig. 1. The calorimeter consists of 12 layers of iron producers, each of 11—12 cm thickness, nine layers of proportional chambers (total 36 chambers), and six layers (total 22 chambers) of visual spark chambers. The total thickness of iron producers is 1.4 m (1 100 g cm^{-2}). A more detailed description of the calorimeter has been published.[9] The purpose of the calorimeter is to study muon interactions in the energy region from several tens of GeV to several TeV. Experimental results have been published[15] for electromagnetic interactions of muons and will be reported[16] elsewhere for nuclear interactions of muons.

B. Trigger system

All the MUTRON instruments are triggered by a signal derived from single muon passages through four layers of the MWPC's having 134×230-cm^2 effective area and the space resolution of 2.4 cm. Such a selection is done by the MWPC matrix coincidence system and only muons of momentum greater than 90 GeV/c are accepted. This decision logic is called the magnet-spectrometer trigger.

In a large-scale magnet spectrometer such as MUTRON, the number of background triggers by air showers is larger than that of incoming muons. The ratio of single muons with high momentum ($\gtrsim$90 GeV/c) to the air-shower background was found to be ~0.05 for the MUTRON spectrometer. Accordingly, for reducing the air-shower background, the antishower selection circuit is used. Also, the location of the site of the MUTRON is greatly affected by background γ rays from the nearby Electron Synchrotron of the Institute for Nuclear Study (INS) of Tokyo University. In order to prevent triggers of MUTRON from this effect, the gate of trigger logic was closed for about 7.8 ms for each of the Electron Synchrotron cycles (21 cycles s^{-1}). The rate of the magnet-

TABLE I. Main characteristics of the MUTRON spectrometer.

Solid-iron magnet	$600\times240\times400$ $cm^3\times2$ (405 + 402 tons)
Deflection power	$\int B\,dl=(66$ kG m$)\times2$
Scattering effect	$\frac{\langle\theta\rangle_{\text{scatt}}}{\langle\theta\rangle_{\text{mag}}}\simeq0.11$
Maximum detectable momentum (maximum value)	22 TeV/c
Collecting power	1360 cm^2 sr reduced to 1280 ± 20 cm^2 sr
Zenith angle	86°—90°
Azimuthal angle	325.4 ± 15.0 (northwest) 145.4 ± 15.0 (southeast)
Detectors	16 multiwire proportional counters 48 double-gap wire spark chambers 4 time-of-flight scintillation counters

spectrometer trigger was approximately 0.7 per minute.

Whenever the spectrometer is triggered, the coordinates of all sparks fired in the WSC's are sent to the computer memory and the same trigger also initiates the process of reading the output pulse heights of the proportional chambers in the calorimeter into the central processing unit of the computer through a CAMAC system. The trigger also fires the visual spark chambers in the calorimeter, which are photographed by three 70-mm cameras.

Besides the magnet-spectrometer trigger, we have employed an additional trigger for the calorimeter, called the calorimeter trigger. Whenever the proportional chambers of the calorimeter detect the incidence of a large number of particles indicative of a high-energy muon interaction, the calorimeter system is triggered in an identical fashion as by the spectrometer trigger. Some details of the trigger condition are given elsewhere.[9]

C. Track-measuring detectors (wire spark chambers)

20 multiwire proportional chambers for triggering and 48 magnetostrictive WSC's are used to locate the muon trajectory positions in the magnet spectrometers and 36 proportional chambers and 22 visual spark chambers in the calorimeter. The details of these detectors have been described in other papers.[17]

The first run[10] was operated with eight layers of 32 WSC's for the x coordinate. Afterwards each of two layers for x and for y coordinates were added.[11] Accordingly, 48 WSC's constitute 12 layers located near two magnets. One layer is formed by four chambers, two for the upper part of the magnet and the other two for the lower one. As each chamber has two gaps, the spectrometer has 24 measuring points per track, namely 20 points for the x coordinate and four points for the y coordinate.

The position of a spark in the WSC which is fired by an incident muon can be measured by the time difference between the spark signal and a fiducial signal from the chamber. The position is measured by a 10-MHz scalar which is started by the fiducial signal. Two fiducial lines are glued at a distance of 10 mm from each edge of a WSC. The fiducial points are measured by an optical method within an accuracy ± 0.1 mm.

D. Alignment of measuring trays

In spectrometer measurements, it is very important that errors in the alignment of all trays be small. All trays, especially, the WSC's are required therefore to lie in a straight line and parallel to the x-y plane. Accuracies of their horizontal distances are not so important for measurements of particle momenta, so that y and z coordinates of each WSC and MWPC were measured by a long stainless-steel scale. Each WSC has four small feet beneath the chamber and the height of each foot can be adjusted by a screw with a circumferential pitch of 1 mm/360°. The chambers are not fixed very tight, standing by their self-weights of 70 kg (small chamber) of 100 kg (large chamber), as a precaution against earthquakes.

Accuracies of measurements of the x coordinates of each chamber are very important. Four stainless-steel scales of 1st class in JIS (Japan Instruments Standard) were glued on each chamber, which can be read by eye up to 0.1 mm. In order to measure the graduations of these scales, we utilize a Carl Zeiss theodolite Th 2 which provides an accuracy of 1″. The accuracy corresponds to a reading of ~ 0.1 mm at a distance of 22 m, which is almost a full length of the MUTRON spectrometer.

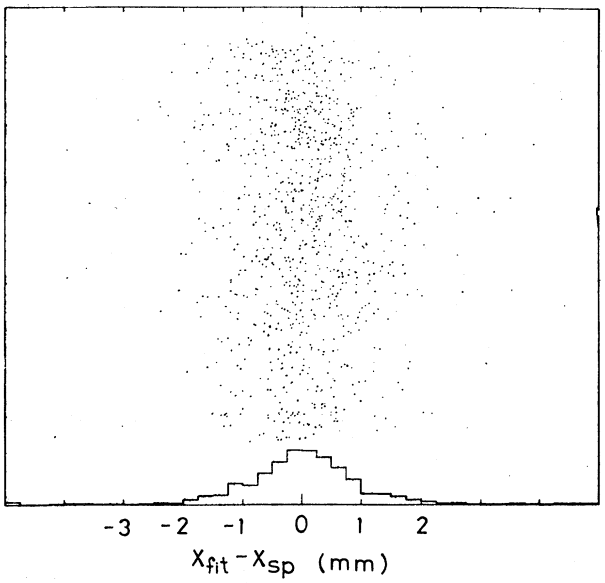

FIG. 2. Distribution of deviations of coordinates of the used sparks in wire spark chambers from a muon trajectory filled by the least-squares method (after completion of the alignment).

After measuring the fiducial scales by the theodolite, a more precise correction of the fiducial wires in each WSC was done by software, by fitting the actual data of zero-field run to straight lines with the least-squares method. After finishing the fine corrections of the position of the fiducial wires, a distribution of deviations of coordinates of used sparks in the WSC's from a muon trajectory, as determined by the least squares method, is shown in Fig. 2. A muon trajectory is accepted only if there are more than eight spark coordinates and if the momentum exceeds 200 GeV/c in order to avoid effects of multiple Coulomb scattering of the muon. The tails of the distribution in Fig. 2 may be attributed to the errors of alignment of all wire WSC's and to a variation of the velocity of a signal pulse transmitted in a magnetorestrictive wire of the WSC's. The position of the fiducial wire was finally adjusted within ± 0.1 mm for the four layers of the chambers between the two magnets and the fiducials for the outer layers were adjusted within ± 0.2 mm. These adjustments have been done and checked for all running data in regular time intervals.

Careful monitoring[18] of positions of all WSC's and MWPC's has been done by the theodolite measurements. However, for the daily monitoring, mechanical gauges have been used. The gauge which can distinguish a minimum deviation of 0.01 mm was set on the top edge of each WSC and MWPC.

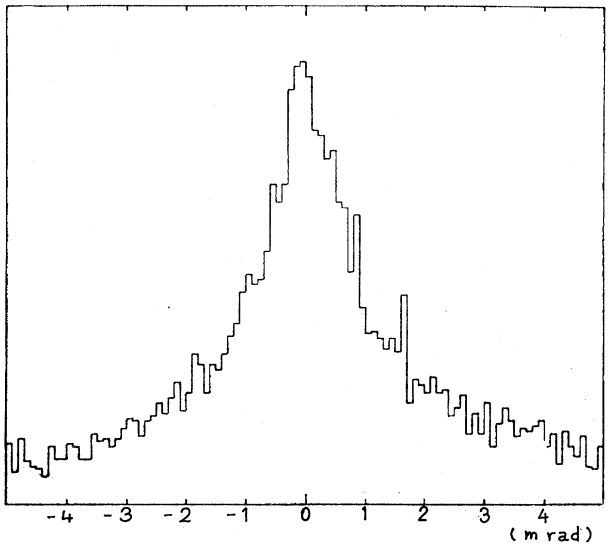

FIG. 3. Distribution of the apparent bending angle of a muon trajectory in zero magnetic field. The MDM can be determined from the most frequent value of the bending angle.

III. CORRECTIONS FOR THE DATA

The raw data on the muon intensities, the muon momentum spectrum and the muon charge ratio, have to be corrected for the spatial resolution and the inefficiency of the individual WSC, muon scattering in the magnet and the calorimeter, the geomagnetic field effect of the earth on the muon trajectory in the atmosphere, and so on. The muon intensities have been measured under the live time which is corrected for the dead time produced by the veto from the INS machine. The dead time needs 10 s for charging up of high-voltage circuits of all WSC's. In this section, these correction factors for the observed results will be discussed and calculated.

A. Maximum detectable momentum (MDM) correction

The definition of MDM is that momentum at which the error on the measurement of momentum is equal to the momentum itself. The error in the determination of the muon momentum is related to overall spatial resolution in all WSC's to be fired by incoming muons. The spatial resolution is a combination of that in the individual WSC. A bending angle of the muon trajectory in zero magnetic field can be handled as one of the muon trajectory in a given magnetic field. For a zero-field run the distribution of bending angles is shown in Fig. 3 for muon trajectories with at least 8 bits in the spark chambers. The uncertainty on the peak position of the distribution, 0.1 mrad, corresponds to a value for MDM of $\sim$40 TeV/c. The tails of the distribution show the effect of low-momentum muons which suffer multiple Coulomb scattering.

The MUTRON spectrometer has 20 measuring points for x coordinates of the WSC's to be fired. However, some chambers may be inefficient. The value of MDM is thus dependent on the number of fired chambers. In Table II, various MDM values are tabulated with respect to the number of fired chambers and the correction factors $R(P)$ are shown as a function of the value of P_μ/P_{MDM} in Table III.

B. Triggering efficiency of MWPC trays

As mentioned in Sec. II B, the trigger logic based on the MWPC trays consists of two steps: the matrix coincidence system for muons with momenta greater than 90 GeV/c, and the anticoincidence particle-selection system for rejecting small side showers. The detection efficiency for incoming muons has been obtained[9] as 0.95 per track by measuring a ratio for the detected numbers of muons around 200 GeV/c for a case of using the triggering system and a case of not using the system (a single fourfold coincidence for MWPC trays).

The detection efficiency might depend on the momentum of the muon. We found that for the lower momentum region, the detection efficiency decreases owing to effects for multiple Coulomb scattering of muons in iron and a large bending of the muon trajectory in the magnetic field. The effect is considered in calculations of $S\Omega$ values. For the higher momentum region, the number of associated particles originated in electromagnetic interac-

TABLE II. Relations of the number of sparks fired at each layer of WSC's to the corresponding values for the MDM.

	Layer number										
	1	9	2	3	4	5	6	7	10	8	MDM (TeV/c)
Number of	2	2	2	2	2	2	2	2	2	2	22.0
data at	2	0	2	2	2	2	2	2	0	2	18.0
each layer	2	2	2	0	2	2	0	2	2	2	17.0
	0	2	2	2	2	2	2	2	2	0	15.9
	1	1	1	1	1	1	1	1	1	1	15.7
	2	0	2	2	2	2	2	2	0	0	13.7
	1	1	1	0	1	1	0	1	1	1	12.0
	1	0	1	0	0	1	0	0	0	1	10.4
	1	0	1	1	1	1	0	1	0	0	9.5
	2	0	2	2	2	2	0	0	0	0	6.5
	2	0	2	2	2	0	0	0	0	0	3.0

TABLE III. Correction factor with MDM effect. $Q(P)$ for the muon momentum spectrum and $R(P)$ for the muon charge ratio. γ: exponent of the observed muon momentum spectrum at oblique zenith angle, CR: muon charge ratio.

	$Q(P)$			$R(P)$		
P_μ/P_{MDM}	$\gamma=2.2$	$\gamma=2.4$	$\gamma=2.6$	CR=1.15	CR=1.25	CR=1.35
7.10	0.1124	0.0730	0.0467	1.1192	1.1192	1.2739
5.64	0.1472	0.0999	0.0670	1.1116	1.1842	1.2555
4.48	0.1920	0.1362	0.0954	1.1024	1.1686	1.2334
3.56	0.2489	0.1844	0.1349	1.0914	1.1500	1.2072
2.82	0.3197	0.2471	0.1885	1.0786	1.1286	1.1771
2.24	0.4052	0.3259	0.2588	1.0642	1.1047	1.1437
1.78	0.5038	0.4206	0.3467	1.0490	1.0796	1.1089
1.42	0.6102	0.5269	0.4495	1.0341	1.0051	1.0752
1.12	0.7150	0.6362	0.5597	1.0210	1.0338	1.0460
0.89	0.8066	0.7366	0.6658	1.0109	1.0176	1.0239
0.71	0.8758	0.8718	0.7568	1.0046	1.0074	1.0100
0.564	0.9201	0.8751	0.8264	1.0014	1.0023	1.0031
0.448	0.9442	0.9114	0.8748	1.0003	1.0005	1.0007
0.356	0.9561	0.9329	0.9064	1.0000	1.0000	1.0001
0.282	0.9623	0.9458	0.9268	1.0000	1.0000	1.0000
0.224	0.9659	0.9538	0.9398	1.0000	1.0000	1.0000
0.178	0.9682	0.9589	0.9482	1.0000	1.0000	1.0000
0.142	0.9695	0.9620	0.9535	1.0000	1.0000	1.0000
0.112	0.9704	0.9640	0.9569	1.0000	1.0000	1.0000
0.089	0.9710	0.9653	0.9590	1.0000	1.0000	1.0000
0.071	0.9713	0.9661	0.9604	1.0000	1.0000	1.0000
0.0564	0.9715	0.9666	0.9613	1.0000	1.0000	1.0000
0.0448	0.9717	0.9669	0.9618	1.0000	1.0000	1.0000
0.0356	0.9717	0.9671	0.9621	1.0000	1.0000	1.0000
0.0282	0.9718	0.9672	0.9624	1.0000	1.0000	1.0000
0.0224	0.9718	0.9673	0.9625	1.0000	1.0000	1.0000

tions of muons in matter increases as the muon momentum increases, so that the detection efficiencies for both regions should decrease. To calculate this effect, a Monte Carlo simulation was done for muons passing through the iron magnets and the atmosphere near the spectrometer. Details of the simulation will be described in Appendix B. The calculated detection inefficiencies per track versus muon momenta are shown in Figs. 4(a) and 4(b).

C. Effect of geomagnetic fields

Although the earth's geomagnetic field is very weak, its effect on the measurement of the muon charge ratio might not be negligible. The longitude and latitude of the location of setting the MUTRON are $\varphi=35.75°$N and $\lambda=139.55°$E. The MUTRON spectrometer accepts muons at zenith angles around 89° and its azimuthal axis is 34° at a direction from north to west with an opening angle of $\pm 15.6°$. Since the passages of muons in the atmosphere becomes very long (a few hundred km), the trajectories will be bent by the geomagnetic field. Kamiya *et al.*[19] have calculated the effect on the muon charge ratio measured by the MUTRON spectrometer. They have obtained correction factors of 1.35 for muons with a momentum of 100 GeV/c coming from the N-W direction and 0.75 for muons of the same energy from the S-E direction.

In the actual measurement by MUTRON, however, the correction factors should be canceled out for N-W and S-E directions each other, because the observations by the MUTRON spectrometer concerns the two directions. For the measured charge-ratio values shown in Fig. 7, thus, only the one with the lowest momentum value (100 GeV/c) was corrected by a factor of 1.01.

IV. DATA ANALYSIS

Candidates for muon events are requested to satisfy the following conditions:

(i) The total number of sparks in the WSC's must be ≥ 7.

(ii) The value of P_{MDM} obtained for each muon candidate must be >8 TeV/c.

(iii) The value of χ^2/ν (ν is the number of degrees of freedom), which is a measure of the quality of a fitted muon track, must be <3.

By these conditions, 5.3 %, 5.9 %, and 6.0 %, of the total number of candidates are rejected for conditions (i), (ii), and (iii), respectively. These conditions are necessary to avoid the selection of some false tracks and events with an accidentally high momentum value. The rejected rates of (i) and (ii) with (5.3 % + 5.9 %) were taken into account in the Monte Carlo—simulated calculation for the effective aperture of the MUTRON spectrometer and the rate of (iii) with 6.0% was added as a correction in the final data as an inefficiency for detecting muons. The χ^2 distri-

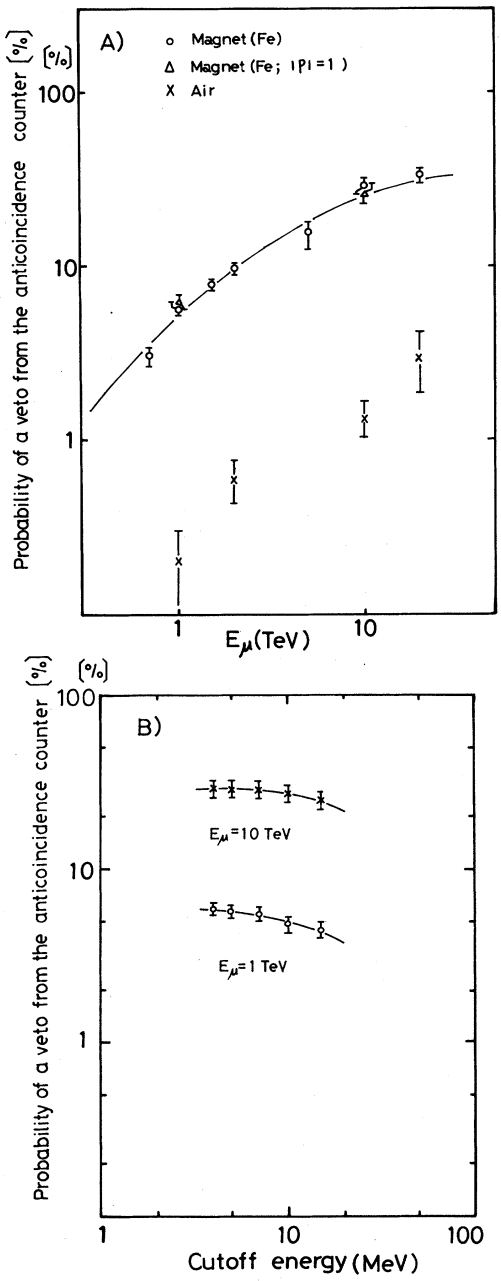

FIG. 4. (A) The detection inefficiency for incident muons which can produce associated secondary particles in matter (magnet, iron, or air), namely, the probability to observe anticoincidence pulses due to this effect. The probability is shown as a function of muon energy. The results in case of $|\rho|=1$ and a flat distribution for $\nu=(\epsilon_+ + \epsilon_-)/E$) are not different and the results in air are negligibly small compared with that in the magnet iron (see Appendix B 1 and B 2). (B) The same probability is given as a variation of the cutoff energy (the smallest energy in the calculations) for the associated particles. There is no strong dependence of the "veto probability" on the cutoff energy.

bution of muon-candidate events will be wider compared to the distribution of Monte Carlo–simulated events for the same degree of freedom. This widening is due to devi-

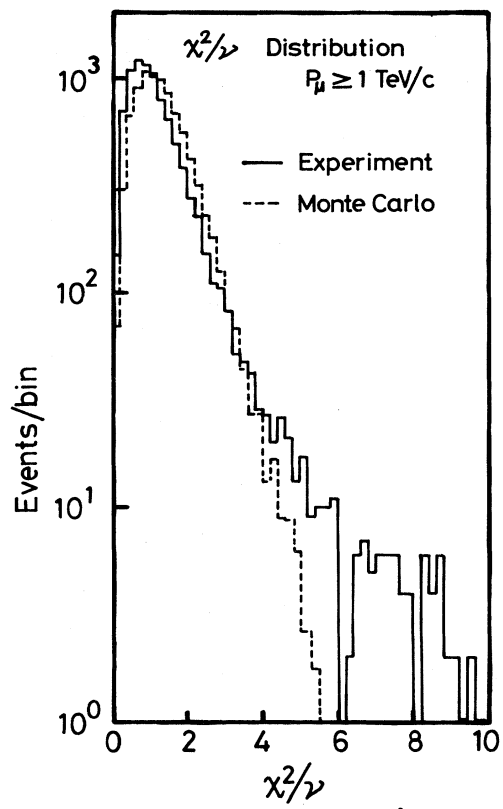

FIG. 5. Comparison of the experiment χ^2/ν distribution of the muon candidates with $P_\mu \geq 1000$ GeV/c with the equivalent distribution calculated by the Monte Carlo method following the three conditions which are given in the text.

ations of the position of sparks from the muon track caused by knock-on electrons in the WSC's. Thus, it is important to accept only the events with $\chi^2/\nu \leq 3$ because the events with $\chi^2/\nu \geq 3$ would have large momentum error. The Monte Carlo simulation for the χ^2/ν distribution of the events following the above three conditions was performed and compared with the experimental χ^2/ν distribution of muon candidates with $P_\mu \geq 1000$ GeV/c in Fig. 5. Both distributions show good agreement except in the large-χ^2/ν region. It shows better agreement than a χ^2 test in the previous work.[10] The experimental distribution shows probabilities of 6.0 % and 2.0 % for the events with $\chi^2/\nu > 3$ and $\chi^2/\nu > 5$, respectively, whereas the calculated ones are 3.8 % for $\chi^2/\nu > 3$ and 0.1 % for $\chi^2/\nu > 5$. The differences between the calculated and experimental distributions are probably caused by misadopted sparks produced by knock-on electrons in the gaps of WSC's. The effects were not taken into account in the Monte Carlo simulation. At present, we could not explain clearly which source of background produced 500 events with $\chi^2/\nu > 5$. But probably small showers associated with and along a muon track may lead to such large-χ^2/ν events.

V. EXPERIMENTAL RESULTS

A. The absolute intensity of cosmic-ray muons

During the operation of MUTRON, some data were selected under good running condition and used to obtain

as the absolute intensity of muons with a momentum larger than 1 TeV/c. The intensity refers to a mean zenith angle of 88.8° covering the angular range from 86° to 90°. Correction factors due to the following effects were introduced:

(a) The MDM correction	0.96±0.02
(b) Correction for the trigger efficiency	1.11±0.06
(c) Correction for the shadowing due to mountains in the aperture of the spectrometer	1.08±0.01
Total correction factor	1.15±0.07

Here, the dead time caused by the INS machine has been already corrected to give the real time of operation. After correcting the measured value, we have obtained for the absolute intensity

$$I_\mu(P_\mu \geq 1 \text{ TeV}/c) = (1.70 \pm 0.10) \times 10^{-7} \text{ cm}^{-1}\text{sr}^{-1}\text{s}^{-1} .$$

The error includes both the statistical error and the systematical uncertainties due to the above correction factors.

B. Momentum spectrum

By using all the corrected data which are then normalized at the absolute intensity for $P_\mu \geq 1$ TeV/c, the measured muon momentum spectrum is obtained as shown in Fig. 6. The effective operating time was 3.39×10^7 s. The vertical scale is expressed by the differential intensity multiplied by P^3. The figure shows the comparison between the momentum spectra measured by the MUTRON and by the DEIS (Kiel—Tel Aviv)[20] spectrometers.[21] While the comparison shows the good agreement within statistical errors, the MUTRON data have better statistics in the high-momentum region. Particularly, the momentum range could be extended beyond 7 TeV/c for a similar zenith-angle region.

C. Charge ratio

In the measurements of the muon charge ratio by a magnet spectrometer, its effective acceptance would be different for positive and negative excitation currents in the magnet. In the MUTRON spectrometer, the effective aperture varies with a combination of the direction of incidence of muons and of positive or negative excitation current. However, we found a nice way to do the measurement of the charge ratio without knowing the different values of the effective aperture.

The observed charge-ratio values are defined by $C_{ob}(+)$ and $C_{ob}(-)$ in the cases of positive and negative excitation currents for the magnets, respectively. The effective aperture Ω^+ for positively charged muons in the case of the positive excitation current is the same as the effective acceptance for negative muons for the negative current. Also the value of Ω^-, which is the effective acceptance for positive muons for the negative current, is equal to the effective acceptance for negative muons in the positive current. If the true charge ratio has a value of C, the following expressions hold:

$$C_{\text{obs}}(+) = C\frac{\Omega^+}{\Omega^-} \text{ for the negative current ,}$$

$$C_{\text{obs}}(-) = C\frac{\Omega^-}{\Omega^+} \text{ for the positive current ,}$$

when the measurements have the same operating hours for both currents. Accordingly,

$$C = [C_{\text{obs}}(+)C_{\text{obs}}(-)]^{1/2} .$$

Thus, we can find the true charge-ratio value without knowing the individual values of Ω^+ and Ω^-.

The charge ratio of cosmic-ray muons obtained by the method are shown with respect to the muon momentum in Fig. 7. The obtained charge-ratio values of 1.251±0.005 and 1.30±0.02 for muons with momenta <600 GeV/c and >600 GeV/c show an increasing ten-

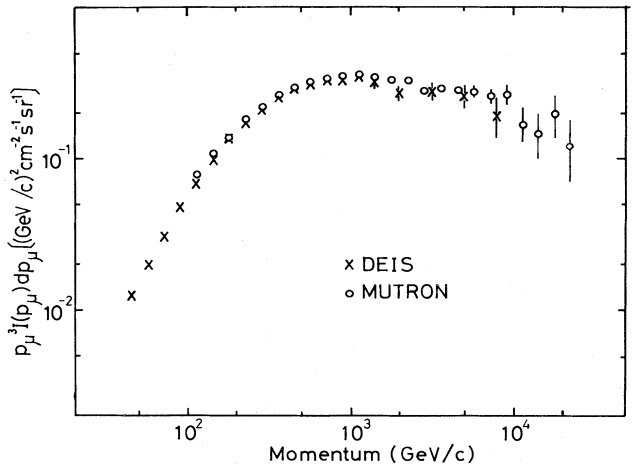

FIG. 6. The measured muon momentum spectrum in absolute value. The vertical scale is expressed by the differential intensity multiplied by p^3. All corrections are included. The figure shows for comparison also the DEIS result (Ref. 19).

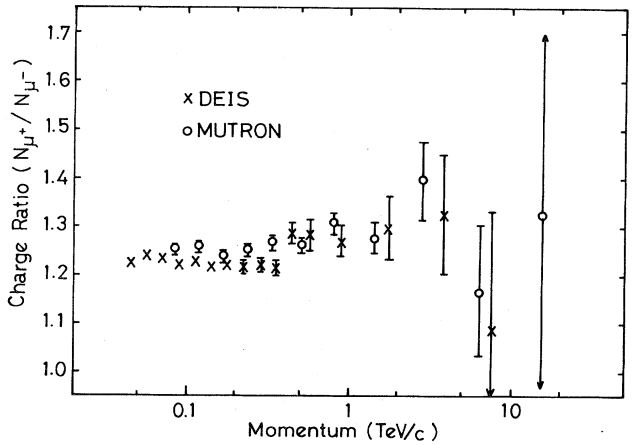

FIG. 7. The muon charge ratio at a zenith angle of 89° as measured by the MUTRON spectrometer. All corrections are included. Also shown are the results of the DEIS group (the average zenith angle 85°).

TABLE IV. The basic data with the momentum bins for both signs of muons. The data are given with all corrections.

Differential muon momentum spectrum				
Momentum bin (GeV/c)	Weighted mean momentum value (GeV/c)	Muon number	Differential intensity $(\text{GeV}/c)^{-1}\,\text{cm}^{-2}\,\text{s}^{-1}\,\text{sr}^{-1}$	Statistical error
100—126	112	70 142	5.69×10^{-8}	$\pm(2.15\times10^{-10})$
126—158	141	60 560	3.99×10^{-8}	$\pm(1.62\times10^{-10})$
158—200	177	50 136	2.41×10^{-8}	$\pm(1.08\times10^{-10})$
200—251	223	40 643	1.60×10^{-8}	$\pm(7.94\times10^{-11})$
251—316	281	31 519	9.88×10^{-9}	$\pm(5.57\times10^{-11})$
316—398	354	23 608	5.90×110^{-9}	$\pm(3.84\times10^{-11})$
398—501	444	16 946	3.37×10^{-9}	$\pm(2.59\times10^{-11})$
501—631	559	11 765	1.88×10^{-9}	$\pm(1.73\times10^{-11})$
631—794	704	7 893	1.02×10^{-9}	$\pm(1.15\times10^{-11})$
794—1 000	886	5 628	5.29×10^{-10}	$\pm(7.05\times10^{-12})$
1 000—1 259	1115	3 114	2.71×10^{-10}	$\pm(4.86\times10^{-12})$
1 259—1 585	1403	1 858	1.31×10^{-10}	$\pm(3.04\times10^{-12})$
1 585—1 995	1766	1 104	6.23×10^{-11}	$\pm(1.88\times10^{-12})$
1 995—2 512	2222	646	2.97×10^{-11}	$\pm(1.17\times10^{-12})$
2 512—3 162	2797	350	1.29×10^{-11}	$\pm(6.90\times10^{-13})$
3 162—3 981	3520	221	6.62×10^{-12}	$\pm(4.45\times10^{-13})$
3 981—5 012	4431	135	3.25×10^{-12}	$\pm(2.80\times10^{-13})$
5 012—6 310	5576	81	1.59×10^{-12}	$\pm(1.77\times10^{-13})$
6 310—7 943	7018	47	7.33×10^{-13}	$\pm(1.07\times10^{-13})$
7 943—10 000	8832	31	3.76×10^{-13}	$\pm(6.75\times10^{-14})$
10 000—12 589	11116	13	1.18×10^{-13}	$\pm(3.27\times10^{-14})$
12 589—15 849	13990	8	5.18×10^{-14}	$\pm(1.83\times10^{-14})$
15 849—19 953	17606	7	3.50×10^{-14}	$\pm(1.32\times10^{-14})$
19 953—25 119	22162	4	1.10×10^{-14}	$\pm(5.50\times10^{-15})$

Integral muon momentum spectrum			
Momentum (TeV/c)	Muon number	Integral intensity $(\text{cm}^{-2}\,\text{s}^{-1}\,\text{sr}^{-1})$	Statistical error
0.10	326 499	6.90×10^{-6}	$\pm(1.21\times10^{-8})$
0.13	256 357	5.42×10^{-6}	$\pm(1.07\times10^{-8})$
0.16	195 797	4.15×10^{-6}	$\pm(9.55\times10^{-8})$
0.20	145 661	3.08×10^{-6}	$\pm(8.07\times10^{-9})$
0.25	105 018	2.22×10^{-6}	$\pm(6.85\times10^{-9})$
0.32	73 499	1.55×10^{-6}	$\pm(5.72\times10^{-9})$
0.40	49 891	1.05×10^{-6}	$\pm(4.70\times10^{-9})$
0.50	32 945	6.95×10^{-7}	$\pm(3.83\times10^{-9})$
0.63	21 180	4.46×10^{-7}	$\pm(3.06\times10^{-9})$
0.79	13 287	2.79×10^{-7}	$\pm(2.42\times10^{-9})$
1.00	7 659	1.70×10^{-7}	$\pm(1.94\times10^{-9})$
1.26	4 545	1.00×10^{-7}	$\pm(1.48\times10^{-9})$
1.59	2 687	5.87×10^{-8}	$\pm(1.14\times10^{-9})$
2.00	1 583	3.40×10^{-8}	$\pm(8.62\times10^{-10})$
2.51	937	1.96×10^{-8}	$\pm(6.51\times10^{-10})$
3.16	587	1.18×10^{-8}	$\pm(4.97\times10^{-10})$
3.98	366	7.00×10^{-9}	$\pm(3.80\times10^{-10})$
5.01	231	4.04×10^{-9}	$\pm(2.82\times10^{-10})$
6.31	150	2.31×10^{-9}	$\pm(2.08\times10^{-10})$
7.94	103	1.32×10^{-9}	$\pm(1.51\times10^{-10})$
10.00	72	6.97×10^{-10}	$\pm(8.43\times10^{-11})$
12.59	59	3.88×10^{-10}	$\pm(6.97\times10^{-11})$
15.85	51	2.14×10^{-10}	$\pm(4.99\times10^{-11})$
19.95	44	1.17×10^{-10}	$\pm(3.31\times10^{-11})$
25.12	40	6.44×10^{-11}	$\pm(2.26\times10^{-11})$

TABLE IV. (*Continued*).

Momentum bin (GeV/c)	Muon charge ratio Field (+) $\mu(+)$	Field (+) $\mu(-)$	Field (−) $\mu(+)$	Field (−) $\mu(-)$	Charge ratio
71–100	14 438	11 255	13 202	10 970	1.243±0.011
100–141	18 773	14 482	16 673	13 656	1.258±0.010
141–200	17 153	13 333	15 249	12 793	1.239±0.010
200–282	13 627	10 671	12 306	10 027	1.252±0.012
282–398	9 711	7 609	8 857	7 073	1.264±0.014
398–631	7 394	5 840	7 012	5 589	1.260±0.016
631–1 000	3 528	2 770	3 335	2 491	1.306±0.024
1 000–1 995	1 570	1 298	1 642	1 221	1.276±0.034
1 995–3 981	360	251	317	234	1.394±0.083
3 981–10 000	86	55	66	76	1.17±0.14
10 000–25 119	10	5	7	8	1.32±0.49
	86 650	6 769	78 666	64 138	

dency which is statistically significant. The statistical errors in the MUTRON data are smaller than those of the DEIS group above 1 TeV/c and comparable with errors of the Utah measurement[22] done by a different method (see Fig. 11).

Both data of the muon momentum spectrum and the charge ratio are tabulated for each momentum bin in Table IV. The quoted values have been fully corrected for all experimental effects.

VI. DISCUSSION

As seen from Fig. 6, a direct comparison of the MUTRON momentum spectrum can be done only with the results of the DEIS spectrograph. Other measurements cannot be directly compared with the MUTRON result because the measurements were either done at different zenith angles or because of their low MDM values. It is seen from the figure that the momentum spectra of the MUTRON and DEIS spectrometers show good agreement between 100 GeV/c and 7 TeV/c within the statistical errors.

In order to compare to other measurements, we will pursue the following two lines.

A. Production spectrum

To compare our present momentum spectrum at sea level with other measurements, all data will be transformed into the parent muon spectrum at production. Following the Thompson and Whalley expression,[23] which assumes that the muon parents are pions and kaons with production spectra of the form $E^{-\gamma}$, the muon spectrum at sea level is

$$N_\mu(E_\mu,\theta^*)dE_\mu = AW_\mu(E_\mu+\Delta E_\mu)^{-\gamma_\pi}\left[\frac{r_\pi{}^{\gamma_\pi-1}B_\pi\sec\theta^*}{E_\mu+\Delta E_\mu+B_\pi\sec\theta^*}+\left[\frac{K}{\pi}\right]b_r\frac{r_K{}^{\gamma_\pi-1}B_K\sec\theta^*}{E_\pi+\Delta E_\mu+B_K\sec\theta^*}\right]dE_\mu ,$$

ΔE_μ is the muon energy loss from production to the apparatus, and W_μ is the muon survival probability. Also,

$$r_\pi=\frac{m_\pi{}^2+m_\mu{}^2}{2m_\pi{}^2}=0.78,\quad r_K=\frac{m_K{}^2+m_\mu{}^2}{2m_K{}^2}=0.52 ,$$

$$\left[\frac{K}{\pi}\right]=2.4\times0.15 \text{ (Ref. 24)} ,$$

$$B_\pi=r_\pi\frac{m_\pi c^2}{\tau_\pi c}\frac{x}{\rho(x)}=90 \text{ GeV} ,$$

$$B_K=r_K\frac{m_\pi c^2}{\tau_K c}\frac{x}{\rho(X)}=442 \text{ GeV} ,$$

where $b_r=0.635$, the branching ratio of the $K_{\mu2}$ decay mode, θ^* is the zenith angle of muon production, x is the atmospheric depth of production in units of g/cm^2, and $\rho(x)$ is the air density at a depth of x. Considering the average zenith angle $\theta=88.8°$ and $\theta^*=84°$ in the MUTRON spectrometer, ΔE_μ is expressed by

$$\Delta E_\mu=(2.5+3.5\times10^{-3}E_\mu)\times10^{-3}x(84°)$$
$$+3.15(2.0+8\times10^{-3}E_\mu)$$

(E_μ in units of GeV), where $x(84°)=27\,600$ g/cm^2 in the model of the U.S. standard atmosphere.[25] The second term is the energy loss in the material of the MUTRON spectrometer so that 3.15 means a length of one iron magnet and a half thickness of iron producers in the calorimeter. Using these expressions and the present momentum spectrum, we obtain for the exponent of the production meson spectrum

$$\gamma_\pi=\begin{cases}2.73\pm0.02\ (P_\mu\geq1 \text{ TeV}/c;\ \chi^2=18.9,\ \nu=13),\\ 2.71\pm0.05\ (P_\mu\geq4 \text{ TeV}/c;\ \chi^2=4.6,\ \nu=7) .\end{cases}$$

TABLE V. Comparisons of γ_π values obtained from magnetic-spectrometer measurements with those from cascade-shower and range measurements. γ_π: exponent of π, K production spectrum, γ_μ: exponent of muon spectrum at sea level, γ_{cascade}: exponent of cascade-shower spectrum. The results from cascade-shower measurements are subdivided into the groups (indicated by the dotted line). The first group gives spectral indices which are compatible with the results from direct measurements, while the second group gives a flatter spectrum.

Methods	Authors	Energy	Exponent	Zenith angles	Depth underground
Magnet-spectrometer measurement[a]	MUTRON (present)	$E \geq 1$ TeV $E \geq 4$ TeV	$\gamma_\pi = 2.73 \pm 0.02$ $\gamma_\pi = 2.71 \pm 0.05$	86–90°	Sea level
	DEIS (Ref. 20)	$E \geq 1$ TeV	$\gamma_\pi = 2.68 \pm 0.05$	85–90°	Sea level
Range measurement	KGF (Ref. 7)	$0.2 \leq E < 40$ TeV	$\gamma_p = 2.60 \pm 0.05$ (2.5–2.68)	0–60°	750–8000 hg/cm^2
	Utah (Refs. 30 and 26)	Around 10 TeV	$\gamma_\pi = 2.60$–2.64 (Ref. 26)	0–45°	2300–4600 hg/cm^2
	Torino-Frascati (Ref. 32)	$E = 1 \sim 10$ TeV	$\gamma_\pi = 2.7$		50–4300 hg/cm^2
	Mt. Blanc (Ref. 31)	$0.2 < E < 5$ TeV	$\gamma_\pi = 2.453 \pm 0.005$	0–80°	700–5000 hg/cm^2
Shower measurement	MUTRON calorimeter (Refs. 15 and 36)	$1 \leq E \leq 6$ TeV	$\gamma_{\text{cascade}} = 2.60 \pm 0.15$ $= 2.74 \pm 0.19$	44–90°	Sea level
	OCU (Ref. 33)	$0.5 \leq E < 8$ TeV	$\gamma_{\text{cascade}} = 2.5 \pm 0.2$ $\gamma_\pi = 2.67$	0–70°	30 hg/cm^2
	Mizutani *et al.* (Ref. 6)	$1 \leq E \leq 10$ TeV	$\gamma_{\text{cascade}} = 2.7 \pm 0.1$	Set horizontally	10 hg/cm^2
	Moscow Engineering Physics Institute (Ref. 65)	$0.2 \sim 3.0$ TeV	$\gamma_\pi = 2.71 \pm 0.1$	60–90°	Sea level
	Basksan underground scintillation telescope (Ref. 34)	$0.3 \sim 1$ TeV	$\gamma_{\text{cascade}} = 2.7 \pm 0.1$	0–60°	850 hg/cm^2 above
	Artenomovsk 100-ton scintillation detector (Ref. 35)	$0.5 < E < 3$ TeV $3 < E < 10$ TeV	$\gamma_{\text{cascade}} = 2.65 \pm 0.05$ $\gamma_{\text{cascade}} = 2.95 \pm 0.2$		600 hg/cm^2
	Moscow Univ. underground detector (Ref. 39)	$0.3 < E < 5$ TeV	$\gamma_{\text{cascade}} = 2.2 \pm 0.15$	Set at vertical	40 hg/cm^2
	Tbilisi State Univ. underground calorimeter (Ref. 38)	$0.8 < E < 4$ TeV	$\gamma_{\text{cascade}} = 2.25 \pm 0.14$	Set at 45°	130 hg/cm^2
	Tien-Shan underground calorimeter (Ref. 37)	$0.3 < E < 10$ TeV	$\gamma_{\text{cascade}} = 2.13 \pm 0.04$	Set at vertical	20 hg/cm^2 at 3340 m height above sea level

[a]Other various measurements are cited in Fig. 8.

The values for γ_π are improved compared to the previous steep value,[10] owing to better MDM values, more data, and more accurate estimations of correction factors in the present analysis. Values for γ_π obtained from other spectrometer measurements at zenith angles above 80° are compared with the MUTRON values in Fig. 8. From the figure, it seems that all values are consistent with one another within the errors. γ_π shows a slowly increasing tendency with momentum.

Comparisons of these γ_π values obtained from magnet-spectrometer measurements with those from measurements of cascade showers and underground range are compiled in Table V. In the table, the exponent of the integral muon spectrum as obtained from range measurements (γ_μ) is almost the same as the differential γ_π values because the measurements are mainly for $P_\mu \geq 1$ TeV and for the vertical direction. As shown already in Fig. 8, the spectrometer measurements are consistent with each other. However, the shower measurements are inconsistent with each other as can be seen from Table V. The deriva-

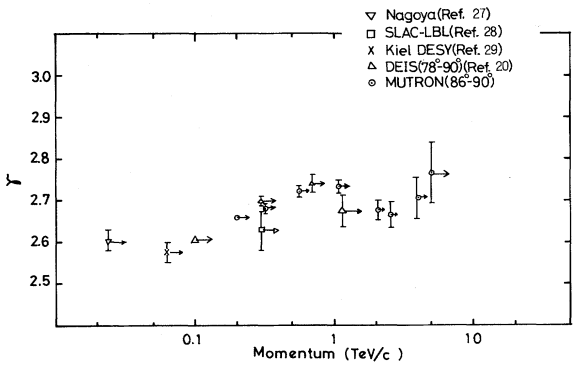

FIG. 8. Comparison of the special indices, γ_π, of π, K spectrum at production obtained from various measurements of muon momentum spectra for oblique direction of incidence.

tion of the muon spectrum from range measurements is affected by uncertainties of muon interactions in rock, in particular inelastic interactions with nuclei in the multi-TeV energy range.[4,26] The spectrometer measurements have also obtained much smaller errors than those of other measurements. Accordingly, we can conclude that the value of γ_π obtained from spectrometers is the most reliable.

B. Comparison with an accurate calculation

From Fig. 8, it seems that the exponent of the parent meson spectrum increases gradually with the muon momentum at production. From this behavior, however, we cannot conclude immediately that the spectral index of cosmic-ray primaries increases with energy, because the simple approximations used are only valid for exact scaling and do not hold at the energies in question. Therefore a more accurate treatment of the particle production spectra and of the interaction process in the atmosphere is necessary. Following this line, many calculations of the muon spectrum at sea level derived from a primary spectrum of shape $AE_0{}^{-\gamma}$ have been done by using a different scaling model for multiplicities of mesons production with increasing cross section. Recent calculations are compared in Table VI, together with various parameters used. In them, Badhwar *et al.*,[40] Murakami *et al.*,[41] and Liland[42] have calculated the muon momentum spectrum for all zenith angles. Their results show a good agreement except that Murakami's model gives a steeper spectrum which decreases faster, compared to the others, above several hundred GeV/c.

At present, Matsuno[43] has done a recalculation following the lines of Komori and Mitsui[44] by using a coherent interaction model for a nucleon-nucleus collision. But he used a different value for the energy-moment term following a recent model[45] for that collision. For the primary cosmic-ray spectrum the two expressions

$$J(E_0)dE_0 = \begin{cases} 1.8E_0{}^{-2.70}dE_0 \,, \\ 2.5E_0{}^{-2.75}dE_0 \end{cases}$$

[E in GeV, $J(E_0)$ in $\mathrm{cm^{-2}sr^{-2}s^{-1}GeV^{-1}}$] were used. The calculated muon energy spectra at a zenith angle of

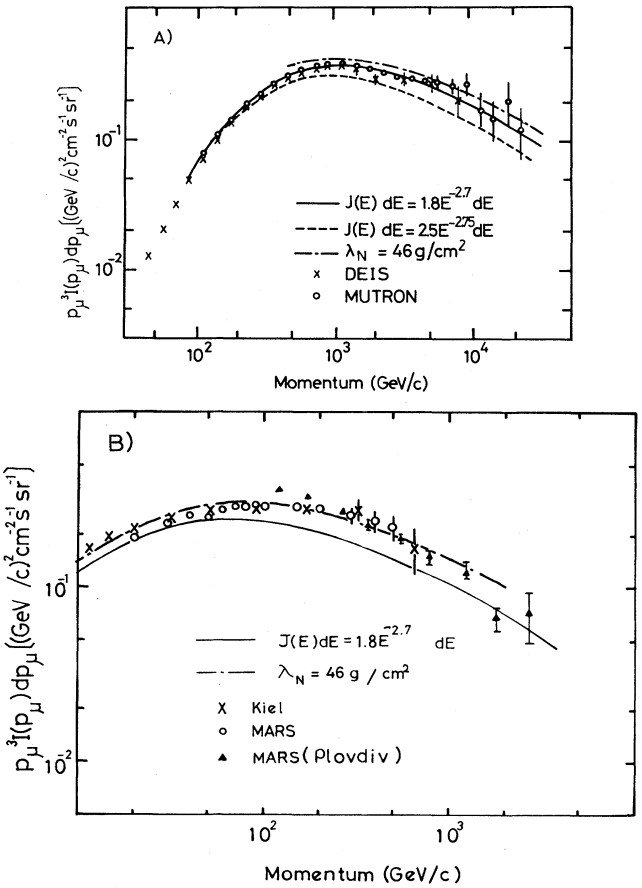

FIG. 9. (A) The MUTRON and DEIS muon energy spectra are compared with the calculated ones at a zenith angle of 89°. The solid line is the result of a calculation based on a primary spectrum of $1.8E^{-2.70}\,dE$ and the dashed curve refers to a primary spectrum of $2.5E^{-2.75}\,dE$. The dashed-dotted curve is calculated using a collision MFP of $\lambda_N = 46$ g/cm^2 which would correspond to an increased abundance of helium nuclei in the primary cosmic-ray spectrum (see text). (B) Comparison of the muon spectrum obtained from an accurate treatment from a primary spectrum of $1.8E^{-2.70}\,dE$ with the Kiel and MARS muon energy spectra for vertical directions. The calculations on the basis of a primary spectrum of $1.8E^{-2.70}\,dE$ can explain the measured muon spectrum at 89° in the absolute scale, however, not for vertical direction. The calculation using $\lambda_N = 46$ g/cm^2 can explain the vertical energy spectrum, but not the one at 89°.

89° are shown in Fig. 9(a), being compared with the MUTRON and DEIS spectra. As seen from the figure, both the spectrometer results give good agreement with a primary cosmic-ray spectrum of ($1.8\ \mathrm{GeV^{-1}\,cm^{-2}\,sec^{-1}\,sr^{-1}}E_0{}^{-2.70}dE_0$) ($E_0$ in GeV). Starting from the same primary spectrum, the muon momentum spectra for the vertical direction has also been calculated by Matsuno. Figure 9(b) shows the result along their measurements from the KIEL[5] and MARS[5] spectrometers. The shape of the spectrum agrees with calculation. However, the experimental results are about 20% higher than the calculated ones as far as the absolute intensities concerned. On the other hand, the calculated results up to

several hundred GeV/c of Murakami *et al.*[41] have been in good agreement with the experimental results for the vertical direction, but above the momentum values decrease faster compared with the experimental ones. Also, the calculated result for 89° was about 20% higher than the experimental results.

The disagreement between the experimental and calculated results for different zenith angles might be caused by any incorrect or oversimplified assumptions in the calculations or some systematic errors of the experimental results in the absolute intensity. Since the experimental results which have been obtained by independent observations for vertical and oblique directions show good agreement with one another, it appears to be rather difficult to attribute the discrepancy to systematical measurement errors. Also, Allkofer *et al.*[20] plotted the data in absolute scale from the Kiel-DESY,[29] Kiel—DEIS—Tel Aviv,[20] and MUTRON spectrometers,[11] for all measured zenith angle bins covering the range from 70° to 90°. All spectra have been fitted to a principally similar calculation based on the conventional muon production using a pion and kaon production distribution of the form $AE^{-\gamma}$.

In the calculation a variation of the intensity of the primary spectrum or a breakdown of the scaling model may give rise to a variation of the muon intensity at sea level, which does not depend on the zenith angle. However, if the collision mean free path (MFP) of primaries becomes shorter (the increasing cross section for interaction), the contribution of the effect to the vertical muon intensity at sea level may be different from that for the oblique direction. In order to evaluate the effect, a calculation with a collision MFP of $\lambda_N = 46$ g/cm^2 has been performed as an extreme case and the muon spectrum at sea level has been obtained for the same primary spectrum of $1.8E^{-2.70}dE$. The value of λ_N corresponds to $\sigma_{pp} = [38.4 + 0.49 \ln^2(s/122)$ mb] (s in GeV^2)[46] at $E_{\rm lab} \approx 150$ TeV and the value corresponds to a MFP of α particles. Very recently, the value of $\sigma_{p\bar{p}}$ has been obtained to be 66 ± 7 mb at a laboratory energy of 155 TeV from the UA4 result at the CERN collider ($\sqrt{s} = 540$ GeV).[47] It seems reasonable to assume $\sigma_{p\bar{p}} = \sigma_{pp}$ for very high energies. According to this formula one would have $\sigma_{pp} = 68$ mb at 155 TeV. This value agrees with the UA4 result within statistical error. The calculated muon spectra for this choice of λ_N are shown by the dashed-dotted line in Figs. 9(a) and 9(b) for comparison with the observed results. From the figures it is clear that the effect of the calculation with $\lambda_N = 46$ g/cm^2 on the muon spectrum is more pronounced for the vertical direction than for 89° because the vertical muon flux at 1 TeV/c is increased by 30%, but that for 89° only by 10%. It is possible to be understood qualitatively with the following explanation. The shorter collision MFP may rise up over all positions of hadron collisions in atmospheres. The variation can increase muon intensities at sea level for the vertical direction owing to increasing probabilities of $\pi, K \rightarrow \mu$ decays in their mesons's longer-traversing atmospheres. For very oblique directions, however, it is difficult to increase the muon intensities because almost all π, K mesons already decay to muons, even in the case with the ordinary MFP. In 1978, Kellogg, Kasha, and Larsen[48] showed a similar disagreement between the measured sea-level muon spectra at 30° and 75° zenith angles in the energy range from 50 to 1700 GeV by using a large rotatable magnetic spectrometer. The results have shown that a conventional production spectrum cannot explain simultaneously the measured intensities at both zenith angles, the intensity at 30° being higher than one at 75° in considering the secθ^* enhancement. From this measured spectra they derived that the fraction of neutrons in the primary flux at energies above 1 TeV/nucleon is more likely to be ~25%, which is larger than observed at lower energies, where it is ~10%. However, recent direct measurements[14] on the primary composition by the JACEE group have presented no evidence that the primaries at energies above 1 TeV are characterized mainly by α particles. But the Australia-Japan-Singapore group[49] has presented that the proton primary intensity at energies > 10 TeV is lower than that which one would obtain from an extrapolation of the low-energy region as measured by Ryan, Ormes, and Balasubrahmanyan.[2] Also, they have measured that the helium primary intensity at energies > 5 TeV/nucleon seems to be higher than the one extrapolated from Ryan *et al.* However, the Australian-Japan-Singapore measurements suffer from a lack of statistics, so that they do not claim their results to be inconsistent with an extrapolation of the results of Ryan *et al.*

Apart from the conventional muon production via decays of pions and kaons, heavy charmed particles which decay in $\lesssim 10^{-12}$ s are produced in the atmosphere. The energy spectrum of muons from heavy-particle decays will have a flatter slope compared to those from π, K decay. Also these "prompt" muons will be isotropically distributed over all zenith angles. Thus at a given zenith angle there will be some energy above which prompt muons will

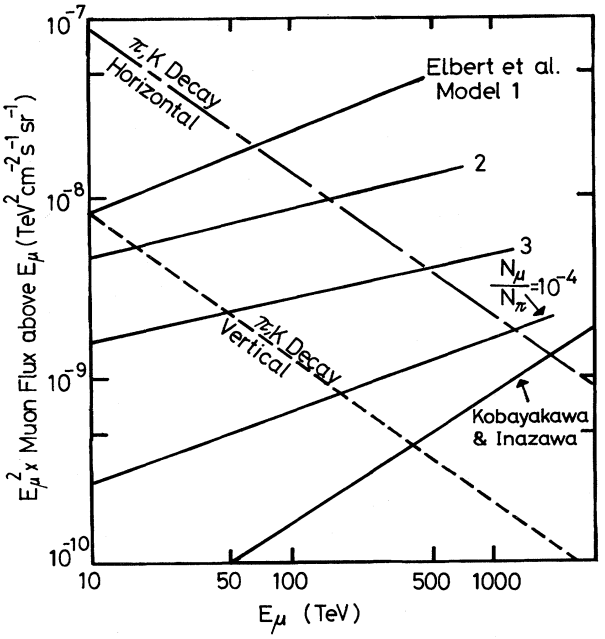

FIG. 10. Prompt (direct) muon flux predicted by various models and compared with the conventional muon flux expected from π, K decays.

dominate and the point of crossover with the conventional muon spectrum occurs at lower energies in the vertical flux than that in the oblique flux. Such a behavior could explain the above discrepancy between the near-vertical and the very oblique muon spectra. In the calculations the contribution of prompt muon production is model dependent and the point of crossover reveals much scatter. The prompt muon flux predicted by some calculations and compared with that from π,K decay, horizontally and vertically, is shown in Fig. 10.[50] The crossover point in the total vertical spectrum is predicted to occur as low as at 10 TeV in a calculation of Elbert, Gaisser, and Stanev[51] and as high as 400 TeV in another calculation of Inazawa and Kobayakawa.[52] In the horizontal spectrum, the former calculation gives the crossover point to be at 60 TeV and the latter one to be at 2000 TeV. Irrespective of the fact that the calculation comes nearer to the truth, the present discrepancy in the absolute intensity sets is already at muon energies as low 10 GeV. Accordingly, the discrepancy is left as an interesting subject for further research.

C. Muon charge ratio

1. Comparison with other measurements

A large number of previous measurements, referred to and shown in Ref. 22, has demonstrated that the charge ratio is essentially constant over the muon energy range from a few GeV to several hundred GeV. A representative value for the near-vertical experiments have been reported by Ayre *et al.*[5] They obtain an average value of 1.285 ± 0.002 over the muon energy range 10—450 GeV. Allkofer, Cartensen, and Dau[5] reported a charge ratio of 1.29 ± 0.02 for muon energies greater than 10 GeV, and Nandi and Sinha[53] a value of 1.28 ± 0.02 for energies greater than 5 GeV. Burnett *et al.*[28] have reported an averaged charge ratio of 1.255 ± 0.007 for energies greater than 25 GeV over a range of zenith angles.

The present experiment is concerned with a measurement of the muon charge ratio in the high-energy range. In Fig. 11, the experimental result on the muon charge ratio of the MUTRON is compared with those at zenith angles $>70°$, i.e., that of the Utah group[22] and that of the world survey data. The world survey data were obtained from measurements of the Nagoya,[27] Kiel-DESY,[29] UCSD,[28] and Yale-BNL[48] spectrometers. The figure shows the good agreement between the MUTRON and the world survey data. The Utah data differ only slightly from others. The charge ratio from the Utah experiment is 1.38 ± 0.02 which has to be compared to 1.29 ± 0.03 for the MUTRON for momenta of >1 TeV/c. The Utah charge-ratio experiment accepted muons with zenith angles between 40° and 90° corresponding to slant depths in excess of 2×10^5 g cm^{-2}, and the muon charge was measured by a spectrometer with a MDM of 100 GeV/c located underground. Accordingly, the individual muon energy estimated from the thickness of the overlying rock which the muon had to penetrate should suffer from large errors attributed to fluctuations of the energy loss in rock. We would say that the direct measurements are more reliable than the Utah results because of the uncertainties of the muon energy loss in the overlying rock.

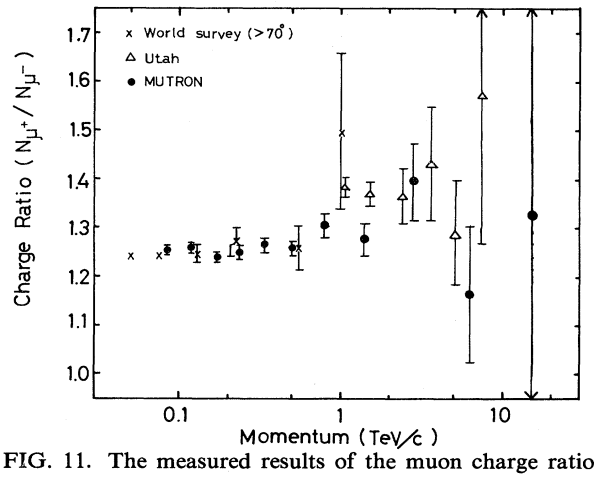

FIG. 11. The measured results of the muon charge ratio of MUTRON are compared with those at zenith angles of $>70°$; those of the Utah group (Ref. 20) and of the world survey data. The world survey data include Nagoya (Ref. 24), UCSD (Ref. 25), Kiel-DESY (Ref. 26), and Yale-BNL (Ref. 45) measurements.

The comparison between the charge ratio of the MUTRON and DEIS spectrometers is shown in Fig. 7. Both data sets show good agreement in the momentum range >400 GeV/c, but the DEIS data give a value which is smaller by 0.02 compared to the MUTRON results in the momentum range <400 GeV/c. If the small differences in the charge ratio at 85° and 89° were real, there should be some theoretical reason for it. Namely, a larger value at 85° (DEIS) than the one at 89° (MUTRON) should be expected theoretically. But the difference shown in Fig. 7 is opposite. The DEIS spectrometer is set up in the east-west direction and accepts only the muons coming from the west direction because of the inclination of the spectrometer. The DEIS data, especially in the low-momentum range, therefore, suffer from geomagnetic effects. On the other hand, the MUTRON spectrometer is located in such a way that these geomagnetic effects might cancel (see Sec. V C). The small differences between both charge ratios in the low-momentum range below 400 GeV/c might be attributed to a difference in the corrections.

2. Comparison with calculations

The charge-ratio measurements can be used as a tool to determine the mass composition of primary cosmic rays, using some aspects of high-energy hadron collisions via model calculations. There is a long history of such model calculations. The pioneering calculation has been done by Frazer *et al.*,[54] combining the steeply falling primary cosmic-ray spectrum with the scaling hypothesis for the spectrum of produced secondary particles, which could be correlated with the data of pion production at machine energies. Their calculation has given the value $\mu^+/\mu^-\sim1.56$ at momenta of several hundred GeV/c, which is too high compared with the experimental results of ~1.25 at the same momentum. Adair[55] has shown the calculated muon charge ratio of 1.53 with the similar cal-

TABLE VI. Parameters used in various recent calculations for the muon energy spectrum or charge ratio.

Authors	Hadronic interactions	Primary cosmic-ray spectrum ($cm^{-2}sr^{-1}s^{-1}$ GeV^{-1})	Results
Badhwar and Stephens (Ref. 40)	$E\frac{d^3\sigma_{pp\to\pi X}}{dp^3}=\frac{1}{(1+4m_p{}^2/s)}(1-X_R)q_{\exp}[-BP_T/(1+4mp^2/s)]$	$0.86E^{-2.55}dE$, $1.2\leq E\leq 68$ GeV	Zenith angles for 0°–79°
	$q=(c_1+c_2P_T+C_3P_T{}^2)/(1+4m_p{}^2s)^{1/2}$	$2E^{-2.75}dE$, 68 GeV $\leq E$	
	$E\frac{d^3\sigma_{pp\to KX}}{dp^3}=A(1-X_R)^c\exp(1-BP_T)$	$\frac{n}{p+n}\sim 0.105$	Muon momentum spectra
	$E\frac{d^3\sigma_{pn\to\pi^\pm X}}{dp^3}=\frac{\lambda_{pp}}{\lambda_{pn}}\left[\left[E\frac{d^3\sigma_{pp\to\pi^\pm X}}{dp^3}\right]+\eta f_n\left[E\frac{d^3\sigma_{pp\to\pi^\pm X}}{dp^3}-E\frac{d^3\sigma_{pp\to\pi^\pm X}}{dp^3}\right]\right]$		Muon charge ratio
		$\frac{\alpha}{p}\sim 0.043$	
	η: Charge mixing parameter ~ 0.195 f_n: A rate of neutrons in target nucleus $\lambda_P=90$ g/cm^2, $\lambda_\pi=120$ g/cm^2, $\lambda_K=150$ g/cm^{-2}		
Thompson and Whalley (Ref. 1)	$E\frac{d^3\sigma_{pp\to ax}}{dp^3}=a_1\exp(a_2+a_3x^2+a_4P_T)$ $=a_1\exp(a_2x+a_3x^2+a_4P_1+a_5P_T{}^2+a_6P_T{}^3)$	$(1.73E^{-2.7}+1.3\times10^{-3}E^{-2.0})dE$	Zenith angle 0°
	$\lambda_p=80$ g/cm^2, $\lambda_\pi=100$ g/cm^2, $\lambda_K=150$ g/cm^2	$\frac{n}{p+n}\sim 0.125$	Muon momentum spectra
			Muon charge ratio
Murakami *et al.* (Ref. 41)	$E\frac{d^3\sigma_{NN\to\pi X}}{dp^3}\propto(1-X_R)^4(P_T{}^2+0.86)^{-4.5}$	$[K_P(E+A_p)^{-\gamma}+K_Z(E+A_Z)^{-\gamma}dE]$	Zenith angles for 0°–89°
	$\langle n_{\pi^\pm}\rangle=4.3+1.71\ln S+3.7S^{-1/2}$		
	$E\frac{d^3\sigma_{NN\to\pi X}}{dp^3}\propto(1-X_R)^3\exp(-4P_T)$		Muon momentum spectra
	$\langle n_{K^\pm}\rangle=-1.02+0.24\ln S+1.45S^{-1/2}$		
	$E\frac{d^3\sigma_{\pi N\to\pi X}}{dp^3}=E\frac{d^3\sigma_{NN\to\pi X}}{dp^3}$		
	$\lambda_p=80$ g/cm^2, $\lambda_\pi=100$ g/cm^2, $\lambda_K=150$ g/cm^2		

γ	K_p	A_p	K_Z	A_Z
2.65	1.1	0.53	4×0.0804	8×10^3
2.75	1.74	0.87	4×0.127	0.31

TABLE VI. (*Continued*).

Authors	Hadronic interactions	Primary cosmic-ray spectrum ($cm^{-2}sr^{-1}s^{-1}$ GeV^{-1})	Results
Liland (Ref. 42)	$G_{ij}=\int_0^1 g_{ij}(U)U^{\gamma}dU$ $E/E'=U$, E being the energy of produced particles and E' the energy of the initial particle, $i=p,n$ $j=p,n,\pi^+,\pi^-,K^+,K^-,K_L^0$ $\lambda_0=84$ g/cm^{-2} $\lambda_{0\pi}=114$ g/cm^{-2} $\lambda_{0K}=130$ g/cm^{-2} $\lambda_0=46.5$ g/cm^{-2} For $\gamma=1.70$: $G_{pp}=0.2028+0.2801E^{-1/2}$ $G_{pn}=0.1147-0.0986E^{-1/2}$ $G_{p\pi^+}=0.041\,90+0.006\,55E^{-1/2}$ $G_{p\pi^-}=0.030\,14-0.010\,19E^{-1/2}$ $G_{pK^+}=0.007\,354-0.006\,456E^{-1/2}$ $G_{pK^-}=0.002\,633-0.003\,179E^{-1/2}$ $G_{an}=2.6$ $\sigma_{inel}=\sigma_0[1+\alpha\ln(E/E')]\equiv(E/E_0)^{\beta(E)}$ λ_0,α,E_0 are constants. $\frac{1}{\lambda_N}=\frac{1}{\lambda_0}\left[1+\alpha\ln\frac{E}{E_0}\right]$	$P(E)=C_pE^{-(\gamma+1)}$	Muon momentum spectra $\theta=0°$, $\gamma=1.70$ $\theta=0°$, $\gamma=1.70$ $\theta=80°$ $C_p=1.114$ $\theta=75°$, $\gamma=1.60$ $\gamma=1.70$ $C_p=0.606$ $C_p=1.079$ Muon charge ratio $\gamma=1.70$, $\gamma=1.60$ $\theta=75°$
Matsuno (Ref. 43)	Same as Minorikawa and Mitsui's one (η is calculated by using Ref. 40). $\lambda_p=80$ g/cm^2, $\lambda_\pi=120$ g/cm^2, $\lambda_K=180$ g/cm^2	$1.8E^{-2.7}dE$ $2.5E^{-2.75}dE$	Zenith angles for $0°-89°$ Muon momentum spectra
Minorikawa and Mitsui (Ref. 60)	$E\frac{d^3\sigma_{pp\to\pi X}}{dp^3}=a(1-x)\exp(-bx^2-cP_T)$, $0.1\le x\le 1$ $=d\exp(-ex-fP_T)$, $0<x<0.1$ $E\frac{d^3\sigma_{pp\to\pi X}}{dp^3}=a(1-x)\exp(-bx^2-cP_T)$	$\propto E^{-2.7}dE$ $\frac{n}{p+n}\sim 0.1$	Zenith angles for $0°-89°$ Muon momentum spectra Muon charge ratio

	a	b	c	d	e	f
π^+	93.71	7.726	4.90	154.6	3.511	6.04
π^-	62.69	10.04	4.92	123.6	6.158	5.59
K^+	6.532	4.465	3.97			
K^-	3.449	12.29	3.76			

$\eta=0.1$, $\lambda_p=80$ g/cm^2, $\lambda_\pi=120$ g/cm^2, $\lambda_K=180$ g/cm^2

culation including K-meson contribution. Hoffman[56] and Erlykin, Ng, and Wolfendale[57] have proceeded with more accurate calculations on this line. Adair *et al.*[58] have measured the charge ratio of muons produced by the interaction of 400-GeV proton with thick copper targets and stated that the difference between the charge ratio and the ratio for cosmic-ray muons may be attributed to the quite large neutron/proton ratio in the primary cosmic rays. Ramana Murthy[59] has commented on the discussion. Many investigations,[60] thus, have tried to interpret this difference in various different ways; by changing the scaling formula, changing the mass composition of the primary cosmic rays, introducing an incoherent intranuclear cascade model, or a coherent production model of nucleon-nucleus collisions, the gluon mechanism of particle production in nucleon-nucleus collision, a multiparticle production model, and the successive breakup of heavy primaries. Also the scaling hypothesis alone at ISR energies incorporating the idea of charge-exchange probability between the nucleon inside a nucleus in a collision seems to be favored by many authors.

Some of the most recent calculations are compared in Table VI, where all parameters of reference which have been used are compiled. All calculations were done based on the assumption of a normal composition, which means with a neutron fraction of $\delta=n/(p+n)=0.1-0.13$. The normal composition (the low-energy composition) has been obtained by direct measurements in the energy range of <1 TeV/nucleon. In such calculations of the muon charge ratio at sea level, not only effects of the electric charge of primary particles, but also effects of neutrons contained inside the target nuclei should be taken into account, since any neutrons participating in the interaction will dilute the charge ratio. Thompson and Whalley[1] have given a rather high value of 1.403 for the charge ratio at a muon production energy of 100 GeV without incorporating the effect of target nuclei in their calculation. Therefore, they have normalized their calculated value at the measured one of 1.28 because in the measurement the effect of target nuclei is of course present. Badhwar and Stephens[40] have introduced an exchange parameter η as a quantity describing the effect of target nuclei. Its value is assumed to be $\eta=0.195$ at the energies in question, which is estimated from the experimental results for p-p and p-n collisions at accelerator energies. Minorikawa and Mitsui[61] estimated η to be 0.1 by using nucleon-nucleus interactions which have been obtained from the experimental analysis by Berlad, Dar, and Erlam.[62] The calculations with the exception of Minorikawa and Mitsui were not performed for a zenith angle of 89° which is the accepted average angle by the MUTRON spectrometer. However, the results of the other calculations can be converted to 89° by taking into account the sec θ^* enhancement following Yekutiel's treatment.[63] Then the MUTRON results can be compared with the modified calculations and directly with the calculations of Minorikawa and Mitsui. Figure 12 shows the various theoretical predictions along with data from MUTRON and Utah. The latter have been converted to 89° in the same way. All calculations are in reasonable agreement with each other and reproduce experimental results within their statistical errors.

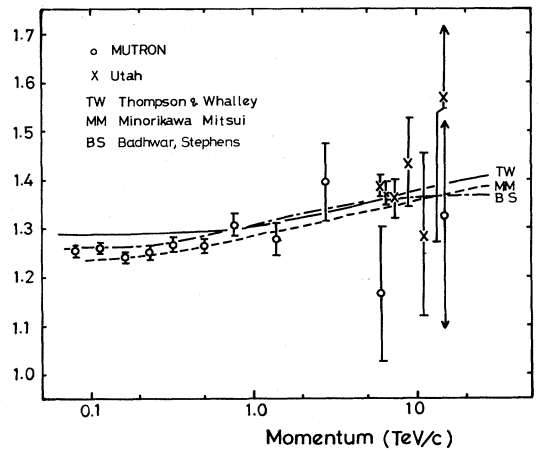

FIG. 12. Comparisons of various experimental results with recent calculations for muon charge ratio.

These calculations for the muon charge ratio were obtained under the assumption of a normal composition of cosmic-ray primaries. On the other hand, we can estimate the fraction of neutrons among primary particles from the measured values of the muon charge ratio at sea level. The results obtained from such a treatment using the calculated values by Badhwar *et al.* are shown in Fig. 13. From the figure an average neutron fraction of 14.9% is obtained for muon energies below 2 TeV. This muon energy range corresponds to primary nucleon energies below 15 TeV/nucleon. Thus, we can conclude that the composition of primary particles in the energy range of 1—15 TeV/nucleon does not change by more than 5% compared to the low-energy composition at energies below 1 TeV/nucleon.

VII. CONCLUSIONS

From the series of MUTRON spectrometer experiments described above, the following conclusions may be drawn.

(1) The sea-level muon momentum spectrum in the momentum range from 100 GeV/c to 20 TeV/c has been measured for zenith angles between 86° and 90° with high statistical accuracy. MUTRON is presently the only experiment in the world which has measured the muon spectrum directly for energies in excess of 7 TeV. The abso-

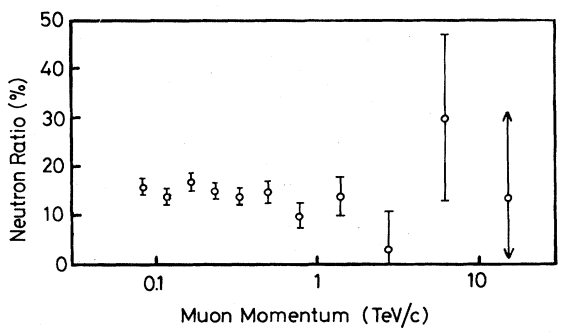

FIG. 13. Fraction of neutrons in primary cosmic-ray particles estimated from the present measurement of the muon charge ratio.

lute muon intensity for momenta above 1 TeV/c at sea level is obtained to be

$$I_\mu(P_\mu \geq 1 \text{ TeV}/c) = (1.70 \pm 0.10) \times 10^{-7} \text{ cm}^{-2}\text{s}^{-1}\text{sr}^{-1}$$

at the mean zenith angle of 88.8°.

(2) From the measured momentum spectrum, the exponent of the π, K-meson production spectra can be obtained on the basis of a simple model. The exponent has been obtained to be 2.73 ± 0.02 for muon momenta above 1 TeV/c.

(3) In a more detailed model calculation starting from a cosmic-ray primary spectrum of

$$J(E)dE = (1.8 \text{ cm}^{-2}\text{s}^{-1}\text{sr}^{-1}\text{GeV}^{-1})\, E^{-2.70} dE \quad (E \text{ in GeV}),$$

the measured muon energy spectrum can be reproduced by using a scaling model for multiplicities of meson production with increasing cross section within the experimental accuracies, although a small discrepancy between the muon intensities for near vertical and near horizontal directions is still left. In particular, no drastic change of the interaction characteristics of high energies (~ 100 TeV) are required to explain the muon momentum spectrum.

(4) The muon charge ratio in the momentum range from 84 GeV/c to 15 TeV/c is measured with high statistical accuracy compared to previous results. The measured values show a very slowly increasing tendency with muon momentum being

$$1.251 \pm 0.005 \text{ for } 100 < p_\mu < 600 \text{ GeV}/c$$

and

$$1.30 \pm 0.02 \text{ for } p_\mu > 600 \text{ GeV}/c .$$

(5) The measured values for the charge ratio can be explained by a calculation using a normal composition of cosmic-ray primaries which has been measured in the low-energy region.

(6) By combining the above conclusions (3) and (5), we may agree that the composition of cosmic-ray primary particles does not change up to ~ 100 TeV. In fact, it is the same as the one obtained by direct measurements for energies below 1 TeV.

ACKNOWLEDGMENTS

This work was supported by a Grant-in-Aid from the Japan Ministry of Education. Dr. Y. Teramoto (High Energy Laboratory) and K. Honda (Yamanashi University) worked during the first period of MUTRON's construction. Also this work has been stimulated by numerous valuable discussions with other MUTRON members. The authors would like to thank Mr. T. Aoki for the help provided during the construction of the apparatus, Mr. N. Fujimaki for his excellent software work, and Mr. H. Inazawa (Kobe University) for his calculations with computer works. We are very grateful to Professor C. Grupen of the University of Siegen for many useful discussions in the preparation of the manuscript. The Computer Room of the Institute for Nuclear Study, University of Tokyo, is thanked for the use of the computer in the analysis of our data.

APPENDIX A: CORRECTION TO THE MOMENTUM SPECTRUM AND THE CHARGE RATIO FOR MULTIPLE COULOMB SCATTERING AND THE FINITE ANGULAR RESOLUTION OF THE SPECTROMETER

A magnetic spectrometer is used to determine the apparent deflection angle and hence equivalent momentum of a single charged particle traversing the instrument. Then, there is an error on the momentum obtained due to multiple Coulomb scattering and the finite angular resolution of the spectrometer. The maximum detectable momentum is usually defined as the momentum at which the corresponding bending angle of the particle is equal to the angular resolution of the spectrometer.

If multiple Coulomb scattering is neglected, the momentum of the particle can be expressed.

$$P = \frac{K}{\theta} , \tag{A1}$$

where K is a constant and θ is the bending angle of the particle. Then, the maximum detectable momentum is given by

$$P_{\text{MDM}} = \frac{K}{\sigma_\theta} , \tag{A2}$$

where σ_θ is the angular resolution of the spectrometer.

The effect of multiple Coulomb scattering (CS) of the muon in the iron magnet causes the bending angle to fluctuate around the angle which corresponds to the muon momentum. The distribution of the bending angle is of Gaussian form with a standard deviation which is 8.0% of the mean bending angle (i.e., the bending angle assuming no scattering) for MUTRON. Namely, as discussed by Rossi and Greisen,[64]

$$\sigma_{\text{CS}} = \frac{\epsilon_{\text{scatt}}}{\sqrt{2}p}\sqrt{T} = \frac{\alpha}{p} , \tag{A3}$$

where $\epsilon_{\text{scatt}} = 21$ MeV and T is the thickness of material in radiation lengths.

For the MUTRON spectrometer, α and K are

$$\alpha = 0.316 \text{ rad GeV} ,$$

$$K = 3.96 \text{ rad GeV} .$$

The total standard deviation for the bending angles including both the scattering effect and the angular resolution is given by

$$\sigma^2 = \sigma_\theta^2 + \sigma_{\text{CS}}^2 . \tag{A4}$$

The probability to find a true momentum P_x as a momentum between P and $P+dP$ is expressed by

$$\begin{aligned} P_{\text{prob}}(P_x, P)dP &= \frac{1}{\sqrt{2\pi}\sigma}\exp\left[-\frac{1}{2}\frac{(\theta-\theta_x)^2}{\sigma^2}\right]d\theta \\ &= \frac{1}{\sqrt{2\pi}\sigma}\exp\left[-\frac{1}{2}\frac{K^2}{\alpha^2}\left[\frac{1}{P}-\frac{1}{P_x}\right]^2\right]\frac{K}{p^2}dP . \end{aligned} \tag{A5}$$

Thus the observed momentum distribution will be

$$N_{\rm obs}(P)dP=\int_{P_x=-\infty}^{\infty}N(P_x)P_{\rm prob}(P_x,P)dP\,dP_x$$
$$=\frac{1}{\sqrt{2\pi}\sigma}\frac{K\,dP}{P^2}\int_{p_x=-\infty}^{\infty}N(P_x)\exp\left[-\frac{1}{2}\frac{K^2}{\sigma^2}\left[\frac{1}{P}-\frac{1}{P_x}\right]^2\right]dP_x \tag{A6}$$

with $N(P_x)dP_x$ being the true momentum distribution.

Now we assume that $N(P)$ has a form of $AC_RP^{(-\gamma+1)}$ for positive muons and $A\mid P\mid^{-(\gamma+1)}$ for negative muons where γ and C_R are constant, although C_R is a slowly increasing function with momentum. Then the observed momentum spectrum of positively charged muons is reduced to

$$N_{\rm obs}(P)dP\mid_{p>0}=\frac{1}{\sqrt{2\pi}\sigma}\frac{K\,dP}{P^2}\int_{-\infty}^{\infty}N(P_x)\exp\left[-\frac{K^2}{2\sigma^2}\left[\frac{1}{P}-\frac{1}{P_X}\right]^2\right]dP_x\Bigg|_{p>0} \tag{A7}$$
$$=\frac{A}{\sqrt{2\pi}\sigma}\frac{K\,dP}{P^2}\left\{C_R\int_0^{\infty}\mid P_x\mid^{-(\gamma+1)}\exp\left[-\frac{K^2}{2\sigma^2}\left[\frac{1}{P}-\frac{1}{P_x}\right]^2\right]dP_x\right.$$
$$\left.+\int_{-\infty}^{0}\mid P_x\mid^{-(\gamma+1)}\exp\left[\frac{K^2}{2\sigma^2}\left[\frac{1}{P}-\frac{1}{P_x}\right]\right]dP_x\right\}\Bigg|_{p>0}$$
$$=A[C_RV_{pp}(P)dP+V_{pn}(P)]dP\ , \tag{A8}$$

where

$$V_{pp}(P)=\frac{1}{\sqrt{2\pi}}\sigma\frac{K}{p^2}\int_0^{\infty}\mid P_x\mid^{-(\gamma+1)}\exp\left[-\frac{K^2}{2\sigma^2}\left[\frac{1}{P}-\frac{1}{P_x}\right]^2\right]dP_x\ ,$$
$$V_{pn}(P)=\frac{1}{\sqrt{2\pi\sigma^2}}\frac{K}{p^2}\int_{-\infty}^{0}\mid P_x\mid^{-(\gamma+1)}\exp\left[-\frac{K^2}{2\sigma^2}\left[\frac{1}{P}-\frac{1}{P_x}\right]^2\right]dP_x\ .$$

With the same procedure the observed spectrum of negatively charged muons is

$$N_{\rm obs}(P)dP\mid_{p>0}=A[C_RV_{pn}(P)+V_{pp}(P)]dP\ . \tag{A9}$$

From Eqs. (A8) and (A9), correction factors $Q(P)$ for the muon momentum spectrum and $R(P)$ for the charge ratio can be calculated by

$$Q(P)=\frac{[N(P)\mid_{p>0}+N(P)\mid_{p<0}]dP}{[N_{\rm obs}(P)\mid_{p>0}+N_{\rm obs}(P)\mid_{p<0}]dP}$$
$$=\frac{A(1+C_R)\mid P\mid^{-(\gamma+1)}}{A[C_RV_{pp}(P)+V_{pn}(P)+C_RV_{pn}(P)+V_{pp}(P)]}$$
$$=\frac{\mid P\mid^{-(\gamma+1)}}{V_{pp}(P)+V_{pn}(P)}\ , \tag{A10}$$

$$R(P)=\frac{N(P)\mid_{p>0}}{N(P)\mid_{p<0}}\frac{N_{\rm obs}(P)\mid_{p<0}}{N_{\rm obs}(P)\mid_{p>0}}$$
$$=C_R\frac{C_RV_{pn}+V_{pp}}{C_RV_{pp}+V_{pn}}\ . \tag{A11}$$

After progressive calculations of the expressions for (A10) and (A11), we find that both $Q(P)$ and $R(P)$ become functions which depend only on the ratio $P/P_{\rm MDM}$ in the high-momentum region $P\geq P_{\rm MDM}/10$. In the low-momentum region $p<P_{\rm MDM}/10$, it is shown from the result in Fig. 14 that both correction factors are constant. Thus observed data may be corrected by using the value

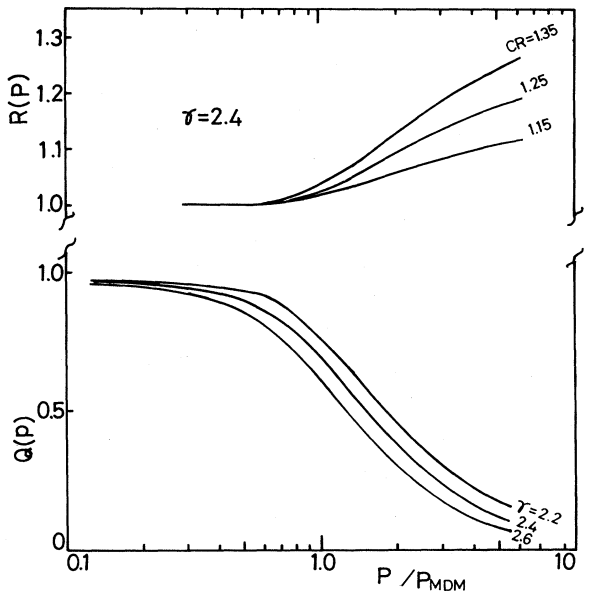

FIG. 14. The correction factors $Q(P)$ for the muon momentum spectrum and $R(P)$ for the muon charge ratio are shown as a function of $P/P_{\rm MDM}$. γ: the exponent of the muon momentum spectrum at 89°, CR charge ratio for a muon momentum spectrum with $\gamma=2.4$ (because the muon momentum spectrum at 89° has the exponent owing to energy loss of muons in atmospheres).

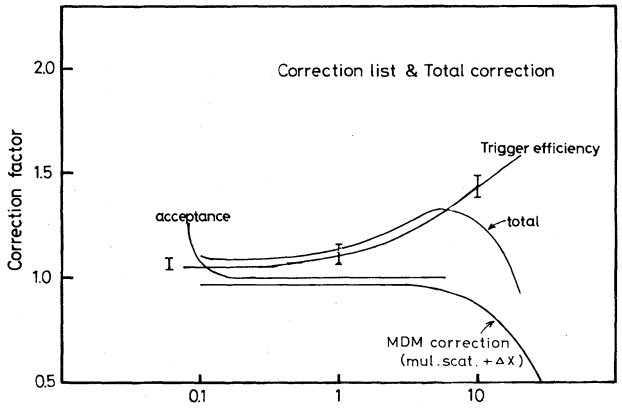

FIG. 15. Momentum dependences of various correction factors. Total correction factor = (MDM correction factor) × (triggering efficiency) × (acceptance).

P/P_{MDM} rather than P and P_{MDM}, respectively.

The results of numerical calculation are shown in Table III and Fig. 14. The momentum dependences of various correction factors are shown in Fig. 15.

APPENDIX B: MONTE CARLO SIMULATION TO EVALUATE THE CORRECTION DUE TO REJECTION OF MUON EVENTS WITH ASSOCIATED PARTICLES BY ANTICOINCIDENCE

In order to evaluate the probability of event rejection which is caused by so-called anticoincidence for a number of particles, a Monte Carlo simulation for muons passing through MUTRON was done. The detection efficiency of the overall MUTRON trigger system including the anticoincidence decreases for low-energy muons due to the effects of Coulomb scattering of the muon in matter (magnet iron and detectors). It also decreases for high-energy muons because of associated particles originating in electromagnetic interactions of muons in matter. The elementary processes considered in this simulation and the procedure utilized in this simulation are described below.

1. Differential probabilities for muon interactions

(a) Knock-on process. The differential probability[64] per $\mathrm{g\,cm^{-2}\,GeV}$, $\Phi(E,E')dE'$ is given as

$$\Phi(E,E')dE'=2\pi N_A r_e{}^2\frac{Z}{A}\times m\frac{dE'}{E'^2}\left[1-\frac{E'}{E'_{\max}}+\frac{1}{2}\left[\frac{E}{E+\mu}\right]^2\right],$$

$$E'_{\max}=\frac{2mE^2}{2mE+\mu^2},$$

where E is the energy of the incident muon (in GeV), E' is the energy of knock-on electron (in GeV), m and μ are the masses of electron and muon, respectively (in GeV), r_e is the classical electron radius, N_A is Avogadro's number, and Z and A are the atomic and mass numbers of the material.

(b) Bremsstrahlung process. The differential probability per $\mathrm{g\,cm^{-2}\,GeV}$, $\Phi(E,E')dE'$, is given as[65]

$$\Phi(E,E')dE'=\alpha N_A\frac{Z^2}{A}r_e{}^2\left[\frac{m}{\mu}\right]^2\frac{dE'}{E'}F(E+\mu,v),$$

$$v=\frac{E'}{E+\mu},$$

and

$$F(E+\mu,v)=4[1+(1+v)^2-\tfrac{2}{3}(1-v)]\times\ln\left[\frac{\frac{2}{3}A\frac{\mu}{m}Z^{-2/3}}{1+\frac{A\sqrt{e}}{2}\frac{\mu^2}{E}\frac{v}{1-v}Z^{-1/3}}\right],$$

where α is the fine-structure constant and the other parameters are the same as those in the knock-on process.

(c) Direct electron-pair production process. The differential cross section $\sigma(E,\nu,\rho)d\nu\,d\rho$ is given by

$$\sigma(E,\nu,\rho)d\nu\,d\rho=\frac{2}{3\pi}(Z\alpha r_e{}^2)\times\frac{1-\nu}{\nu}\left[\phi_e+\left[\frac{m}{\mu}\right]^2\phi_\mu\right]d\nu\,d\rho,$$

where

$$\nu=\frac{\epsilon_+ +\epsilon_-}{E},\quad \rho=\frac{\epsilon_+ -\epsilon_-}{E},$$

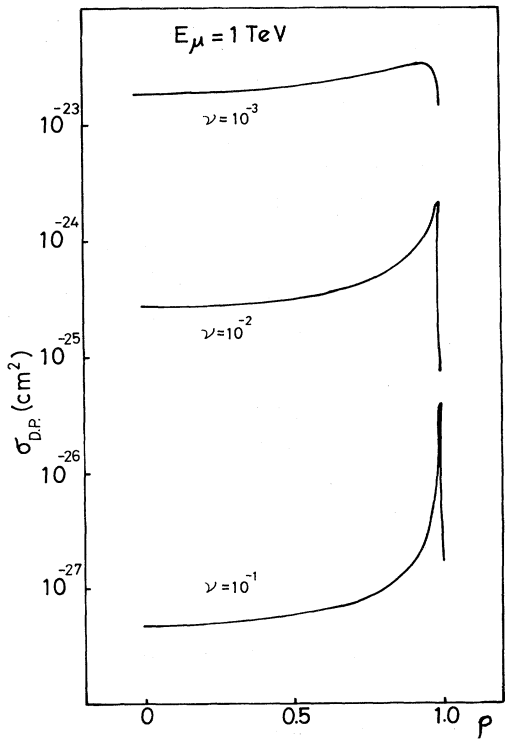

FIG. 16. Cross section for electron pair production by muons of energy 1 TeV for different ρ values. The cross section varies with ρ for different ν values.

and ϵ_+ and ϵ_- are the energy of position and electron, respectively. The other notations ϕ_e and ϕ_μ are taken from a paper of Kokoulin *et al.*[66] As both of the notations are given by long expressions, we do not quote them here.

2. Treatment for muon interactions

All differential probabilities except for the ρ dependences in direct pair production were completely used in this simulated calculation. The expression for the ρ dependence in the pair production has a sharp peak around $\rho=1$ and $\rho=-1$, and the shape of the peaks change with different values of ν (see Fig. 16). The present simulation was done for the two extreme cases. In the first case a flat distribution was used and in the other case a sharp peak was assumed to be at $\rho=1$ and $\rho=-1$. The results of both approximations agree with each other in the range from $E_\mu=1$ to 10 TeV within the limit of calculated errors. Thus the simulated calculation was done only for the assumption of a flat distribution for other values of muon energies, and moreover, it was simplified in the sense that secondary particles produced by a muon such as electrons, positrons, or photons are emitted along the trajectory of the parent muon without any recoil of the muon.

3. Electromagnetic cascades

The processes in electromagnetic cascade showers treated in the simulation are bremsstrahlung, pair production, Compton scattering, multiple Coulomb scattering and a constant energy loss. The cross sections for those processes and the simulation procedure was done following the work of Messel and Crawford.[67] The energy threshold of secondary particles was taken to be 4 MeV. The simulation was applied for muon trajectories and trajectories of associated electrons contained in the cascade, which are bent in the field of the iron magnets.

The results of the electromagnetic cascade simulations are shown in Fig. 17, where also a comparison is made with Greisen's one-dimensional cascade curves which are calculated in Approximation B.

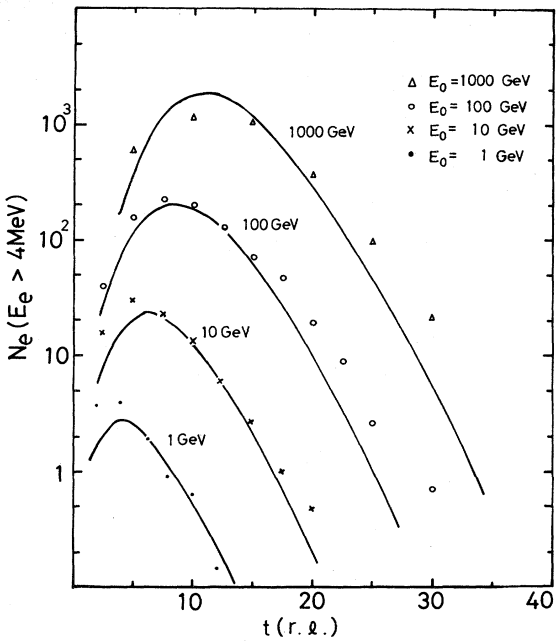

FIG. 17. Comparison of the electromagnetic cascade simulation at various energies with Greisen's one-dimensional cascade curves in Approximation B defined by Rossi and Greisen (Ref. 64).

4. Simulation procedure and results

At first a position, a direction, and a momentum of each charged secondary particle generated from the bottom of the iron blocks or from the atmosphere near the spectrometer were obtained by the simulation for the incident muon which was assumed to pass through the center of each detector. Using the results, the probability that a certain number of the charged secondary particles are rejected by the anticoincidence system was estimated in its variation on the energy of the incident muon. The obtained results for the iron magnet and for the air are shown in Fig. 4(A). A similar result for the iron magnet under another assumption (a sharp peak at $\rho=+1$ and -1) is also shown in the same figure for comparison. It is obvious from the figure that both approximations on the ρ dependence give the same result.

[1]M. G. Thompson and M. R. Whalley, J. Phys. G 3, 97 (1977); O. C. Allkofer, K. Carstensen, W. D. Dau, and H. Jokisch, Phys. Rev. Lett. 41, 832 (1978).

[2]M. J. Ryan, J. F. Ormes, and V. K. Balasubrahmanyan, Phys. Rev. Lett. 28, 985 (1972); N. L. Grigorov, Yu. V. Gubin, I. D. Rapport, I. A. Savenko, B. M. Yakovlev, V. V. Akimov, and V. E. Nesterov, Yad. Fiz. 11, 1058 (1970) [Sov. J. Nucl. Phys. 11, 588 (1970)].

[3]A. D. Erlykin, K. K. Ng, and A. W. Wolfendale, J. Phys. A 7, 2059 (1974); V. G. Kirillov-Ugryumov, A. A. Petrukhin, and V. V. Shestakov, in *Proceedings of the Fourteenth International Conference on Cosmic Rays, Munich 1975,* edited by Klaus Pinkau (Max-Planck-Institut, München, 1975), Vol. 6, p. 1943; P. K. Grieder, Nuovo Cimento 7, 1 (1977).

[4]G. L. Cassiday, Phys. Rev. D 3, 1109 (1971); L. Bergamasco and P. Picchi, Nuovo Cimento 3B, 134 (1971); Y. Minorikawa, T. Kitamura, and K. Kobayakawa, Nuovo Cimento 4C, 471 (1981).

[5]O. C. Allkofer, K. Carstensen, and W. D. Dau, Phys. Lett. 36B, 425 (1971); C. A. Ayre, J. M. Baxendale, C. J. Hume, B. C. Nandi, M. G. Thompson, and M. R. Whalley, J. Phys. G 1, 584 (1975).

[6]K. Mizutani, A. Misaki, T. Shirai, Z. Watanabe, M. Akashi, and Y. Takahashi, Nuovo Cimento 48A, 429 (1978); M. A. Ivanova, L. A. Kuzmichev, K. V. Mandritskaya, E. A. Osipova, I. V. Rakobolskaya, N. V. Sokolskaya, A. Ya. Varkovitskaya, G. T. Zatsepin, and V. I. Zatsepin, in *Sixteenth International Cosmic Ray Conference, Kyoto, 1979, Conference Papers* (Institute of Cosmic Ray Research, University of Tokyo, Tokyo, 1979), Vol. 10, p. 33.

[7]M. R. Krishnaswamy, M. G. K. Menon, V. S. Narasimham, N. Ito, S. Kawakami, and S. Miyake, in *Proceedings of the Fifteenth International Conference on Cosmic Rays, Plovdiv, 1977,* edited by B. Betev (Bulgarian Academy of Sciences, Sofia, 1977), Vol. 7, p. 85; M. F. Crouch, P. B. Landecker, J. F. Lathrop, F. Reines, W. G. Sandie, H. W. Sobel, H. Coxell, and J. P. F. Sellschop, Phys. Rev. D 18, 2239 (1978).

[8]T. Kitamura, in *17th International Cosmic Ray Conference, Paris, 1981, Conference Papers* (Centre d' Etudes Nucleaires, Saclay, 1981), Vol. 13, p. 361.

[9]S. Higashi, K. Honda, S. Ozaki, T. Takahashi, Y. Teramoto, T. Kitamura, K. Mitsui, S. Miyake, Y. Muraki, I. Nakamura, Y. Ohashi, A. Okada, S. Iida, Y. Kamiya, Y. Kawashima, H. Shibata, K. Kobayakawa, S. Mikamo, and Y. Minorikawa, Nucl. Instrum. Methods 150, 387 (1978); K. Mitsui, A. Okada, T. Kitamura, S. Miyake, Y. Muraki, Y. Ohashi, S. Ozaki, and S. Mikamo, *ibid.* 169, 96 (1980).

[10]Y. Muraki, Y. Ohashi, T. Katamura, K. Mitsui, S. Miyake, A. Okada, P. V. Ramana Murthy, K. Honda, Y. Kawashima, T. Takahashi, Y. Teramoto, S. Higashi, S. Ozaki, I. Nakamura, Y. Kamiya, S. Iida, K. Kobayakawa, H. Shibata, Y. Minorikawa, and S. Mikamo, Phys. Rev. Lett. 43, 974 (1979); Y. Muraki, Y. Kawashima, T. Kitamura, S. Matsuno, K. Mitsui, S. Miyake, Y. Ohashi, T. Suda, P. V. Ramana Murthy, S. Higashi, K. Honda, S. Ozaki, T. Takahashi, Y. Teramoto, Y. Kamiya, I. Nakamura, K. Kobayakawa, H. Shibata, Y. Minorikawa, and S. Mikamo, Phys. Rev. D 28, 40 (1983).

[11]Y. Kawashima, T. Kitamura, S. Matsuno, K. Mitsui, Y. Muraki, Y. Ohashi, A. Okada, T. Suda, Y. Minorikawa, K. Kobayakawa, Y. Kamiya, I. Nakamura, and T. Takahashi, in *17th International Cosmic Ray Conference, Paris 1981, Conference Papers* (Ref. 8), Vol. 7, p. 16.

[12]A. D. Erlykin, L. K. Ng, and A. W. Wolfendale, J. Phys. A 7, 2059 (1974); T. K. Gaisser, J. Geophys. Res. 79, 2281 (1974).

[13]UA1 Collaboration, Phys. Lett. 107B, 320 (1981); UA5 Collaboration, *ibid.* 107B, 315 (1981).

[14]J. C. Gregory, T. Ogata, T. Saito, R. Holynski, A. Jurak, W. Wolter, B. Wosiek, S. Dake, M. Fuki, T. Tominaga, E. M. Friedlander, H. H. Heckman, R. W. Huggett, J. J. Lord, W. V. Jones, Y. Takahashi, T. A. Parnell, O. Miyamura, T. H. Burnett, J. J. Lord, R. J. Wilkes, T. Hayashi, J. Iwai, and T. Tabuki, in *17th International Cosmic Ray Conference, Paris, 1981, Conference Papers* (Ref. 8), Vol. 9, p. 154; Phys. Rev. Lett. 50, 2062 (1983), the next proposal of the JACEE group.

[15]K. Mitsui, A. Okada, Y. Kawashima, T. Kitamura, S. Matsuno Y. Muraki, Y. Ohashi, T. Suda, T. Takahashi, S. Higashi S. Ozaki, I. Nakamura, Y. Kamiya, K. Kobayakawa, H. Shibata, Y. Minorikawa, and S. Mikamo, in *Sixteenth International Cosmic Ray Conference, Kyoto, 1979, Conference Papers* (Ref. 6), Vol. 10, p. 29; Nuovo Cimento 73A, 209 (1983); 73A, 235 (1983).

[16]A. Okada, K. Mitsui, Y. Kawashima, T. Kitamura, Y. Muraki, Y. Ohashi, and T. Takahashi, in *17th International Cosmic Ray Conference, Paris, 1981, Conference Papers* (Ref. 8), p. 355; Fortschr. Phys. (to be published).

[17]T. Kitamura, K. Mitsui, Y. Muraki, A. Okada, Y. Ohashi, and I. Nakamura, in *Proceedings of the Fourteenth International Conference on Cosmic Rays, Munich, 1975* (Ref. 3), Vol. 9, p. 3301.

[18]Rei Ruo Shen and T. Kitamura, Institute for Cosmic Ray Research, University of Tokyo, Report No. 84-80-6, 1980 (unpublished).

[19]Y. Kamiya, S. Iida, and S. Shibata, in Proceedings of the Asian Cosmic Ray Conference, Hong Kong (unpublished), p. 133.

[20]O. C. Allkofer, K. Carstensen, G. Bella, W. D. Dau, H. Jokisch, G. Kemeke, Y. Oren, and R. C. Uhr, in *Sixteenth International Cosmic Ray Conference, Kyoto, 1979, Conference Papers* (Ref. 6), Vol. 10, p. 50; in *17th International Cosmic Ray Conference, Paris, 1981, Conference Papers* (Ref. 8), Vol. 10, p. 321.

[21]The DEIS spectrometer constructed by a Kiel-Tel Aviv collaboration is the second largest spectrometer with a MDM of 7 TeV/c for a mean zenith angle of 85° covering 78° to 90°.

[22]G. K. Ashley II, J. W. Keuffel, and M. O. Larson, Phys. Rev. D 12, 20 (1975).

[23]M. G. Thompson and M. R. Whalley, J. Phys. G 1, L48 (1975).

[24]The factor of 2.4 is evaluated from differences in collision mean-free paths for π and K mesons and different momentum spectra for decay muons from both mesons. 0.15 is the production ratio for π and K in collisions with air nuclei of primary cosmic rays.

[25]K. Maeda, Fortschr. Phys. 21, 113 (1973).

[26]K. Kobayakawa, in *Proceedings of the Thirteenth International Conference on Cosmic Rays, Denver, 1973* (Colorado Associated University Press, Boulder, 1973), Vol. 5, p. 3156.

[27]S. Iida, Nuovo Cimento 26B, 559 (1975).

[28]T. H. Burnett, J. J. Lamay, G. E. Masek, T. Maung, E. S. Mitler, H. H. Ruderman, and W. Vernon, in *Proceedings of the Thirteenth International Conference on Cosmic Rays, Denver, 1973* (Ref. 26), Vol. 3, p. 1764; Phys. Rev. Lett. 30, 937 (1973).

[29]H. Jokisch, K. Carstensen, W. D. Dau, H. J. Meyer, and O. C. Allkofer, Phys. Rev. D 19, 1368 (1979).

[30]G. L. Cassiday, P. C. Gilbert, and D. M. White, Phys. Rev. 27, 164 (1971).

[31]W. R. Sheldon, J. R. Benbrook, N. M. Duller, E. G. Cantrell, A. R. Bager-Bachi, Gilbert Vedeene, and Cleude Dunet, Phys. Rev. D 17, 114 (1978).

[32]L. Bergamasco and B. D'Ettore Piazzoli, Nuovo Cimento 4B, 59 (1971).

[33]S. Higashi, F. Kajino, M. Nakashita, S. Ozaki, T. Takahashi, and S. Yamamoto, in *17th International Cosmic Ray Conference, Paris, 1981, Conference Papers* (Ref. 8), Vol. 7, p. 71; F. Kajino, Ph.D thesis, Osaka City University, 1982.

[34]Yu. M. Andreyev, V. N. Bakatanov, A. E. Chudakov, G. P. Keydan, N. F. Klimenko, V. Ya. Markov, Yu. F. Novosel'tsev, Yu. V. Sten'kin, and V. I. Stepanov, in *17th International Cosmic Ray Conference, Paris, 1981, Conference Papers* (Ref. 8), Vol. 7, p. 67.

[35]R. I. Enikeev, V. A. Kudryavtsev, A. S. Malgin, O. G. Rhajhskaya, and G. T. Zatsepin, in *17th International Cosmic Ray Conference, Paris, 1981, Conference Papers* (Ref. 8), Vol. 10, p. 359.

[36]K. Mitsui, A. Okada, Y. Kawashima, T. Kitamura, S. Matsuno, Y. Muraki, Y. Ohashi, T. Suda, I. Nakamura, K. Kobayakawa, H. Inazawa, Y. Minorikawa, and S. Mikamo, J. Phys. G 9, 573 (1983).

[37]A. D. Erlykin, A. K. Kulichenko, S. K. Machavariani, and S. I. Nikolsky, in *Proceedings of the Thirteenth International Conference on Cosmic Rays, Denver, 1973* (Ref. 26), Vol. 3, p. 1803.

[38]V. A. Aglamazov, L. D. Gedevanishvili, and I. I. Sakarelidge, in *17th International Cosmic Ray Conference, Paris, 1981, Conference Papers* (Ref. 8), Vol. 7, p. 63.

[39]Yu. N. Bazhutov, N. P. Ilgina, B. A. Khrenov, G. B. Khristiansen, and N. I. Lagutkina, in *17th International Cosmic Ray Conference, Paris, 1981, Conference Papers* (Ref. 8), Vol. 7, p. 59.

[40]G. D. Badhwar and S. A. Stephens, in *Proceedings of the Fifteenth International Conference on Cosmic Rays, Plovdiv, 1977* (Ref. 7), Vol. 6, p. 200; Phys. Rev. D 15, 821 (1977).

[41]K. Murakami, S. Sagisaka, A. Inoue, Y. Mishima, and K. Nagashima, in *Sixteenth International Cosmic Ray Conference, Kyoto, 1979, Conference Papers* (Ref. 6), Vol. 10, p. 70.

[42]A. Liland, Fortschr. Phys. 23, 571 (1975); in *Sixteenth International Cosmic Ray Conference, Kyoto, 1979, Conference Papers* (Ref. 6), Vol. 13, pp. 347 and 353.

[43]S. Matsuno, Ph.D thesis, University of Tokyo, 1982.

[44]H. Komori and K. Mitsui, Nuovo Cimento 4C, 52 (1981).

[45]J. A. Goodman, R. W. Ellsworth, A. S. Ito, J. R. MacFall, F. Siohan, R. E. Streimatter, S. C. Tonwar, P. R. Vishwanath, and G. B. Yodh, Phys. Rev. Lett. 42, 854 (1979).

[46]G. Giacomelli and M. Jacob, Phys. Rev. 55, 1 (1979).

[47]J. G. Rushbrooke, Report No. CERN/EP 82-157, 1982 (unpublished).

[48]R. G. Kellogg, H. Kasha, and R. C. Larsen, Phys. Rev. D 17, 98 (1978).

[49]S. Tasaka, V. D. Hopper, H. Fuki, K. Hoshino, S. Kuramata, K. Niu, K. Niwa, H. Shibuya, Y. Yanagisawa, Y. Maeda, H. Kimura, Y. K. Lim, N. Ushida, and Y. Sato, Phys. Rev. D 25, 1765 (1982).

[50]DUMAND omnibus proposal, 1982 (unpublished), Sec. 2.3.

[51]J. W. Elbert, T. K. Gaisser, and T. Stanev, in *Proceedings of the 1980 DUMAND Symposium, Honolulu,* edited by V. J. Stenger (Hawaii DUMAND Center, Honolulu, 1981), Vol. 1, p. 222.

[52]H. Inazawa and K. Kobayakawa, Prog. Theor. Phys. 69, 1195 (1983).

[53]B. C. Nandi and M. S. Sinha, Nucl. Phys. B40, 289 (1972).

[54]W. R. Frazer, C. H. Poon, D. Silberman, and H. J. Yesian, Phys. Rev. D 7, 1653 (1972).

[55]R. K. Adair, Phys. Rev. Lett. 33, 115 (1974).

[56]H. J. Hoffman, Phys. Rev. D 12, 82 (1975).

[57]A. D. Erlykin, L. K. Ng, and A. W. Wolfendale, J. Phys. A 7, 2059 (1974); 8, L51 (1975).

[58]R. K. Adair, H. Kasha, R. G. Kellogg, L. B. Leipuner, and R. C. Larsen, Phys. Rev. Lett. 39, 112 (1977).

[59]P. V. Ramana Murthy, Cosmic Ray Laboratory, University of Tokyo, Report No. 51-77-10, 1977 (unpublished).

[60]See A. K. Das and A. L. De, J. Phys. G 5, 445 (1979).

[61]Y. Minorikawa and K. Mitsui, in *17th International Cosmic Ray Conference, Paris, 1981, Conference Papers* (Ref. 8), Vol. 10, p. 333.

[62]G. Berlad, A. Dar, and G. Eilam, Phys. Rev. D 22, 1547 (1980).

[63]G. Yekutieli, in *Sixteenth International Cosmic Ray Conference, Kyoto, 1979, Conference Papers* (Ref. 6), Vol. 10, pp. 117 and 123.

[64]B. Rossi and K. Greisen, Rev. Mod. Phys. 13, 240 (1941); B. Rossi, *High Energy Particles* (Prentice-Hall, Englewood Cliffs, New Jersey, 1952).

[65]A. A. Petrukhin and V. V. Shestakov, Can. J. Phys. 46S, 5377 (1968).

[66]R. P. Kokoulin and A. A. Petrukhin, in *Proceedings of the Eleventh International Conference on Cosmic Rays, Budapest, 1969,* edited by P. Gomŏas, Acta Phys. Acad. Sci. Hung. Suppl. 4, 277 (1970); in *Proceedings of the Twelfth International Conference on Cosmic Rays, Hobart, 1971,* edited by A. G. Fenton and K. B. Fenton (University of Tasmania Press, Tasmania, 1971), Vol. 6, p. 2436; R. P. Kokoulin, A. A. Pavlov, A. A. Petrukhin, and V. V. Shestakov, in *Proceedings of the Thirteenth International Conference on Cosmic Rays, Denver, 1973* (Ref. 26), Vol. 3, p. 1797.

[67]H. Messel and D. F. Crawford, *Electron Photon Shower Distribution Function* (Pergamon, New York, 1970).